PAPER • **OPEN ACCESS**

Synthesis of novel coumarin-triazole hybrids and first evaluation of the 4-phenyl substituted hybrid loaded PLGA nanoparticles delivery system to the anticancer activity

To cite this article: Busra Arvas *et al* 2024 *Nanotechnology* **35** 305602

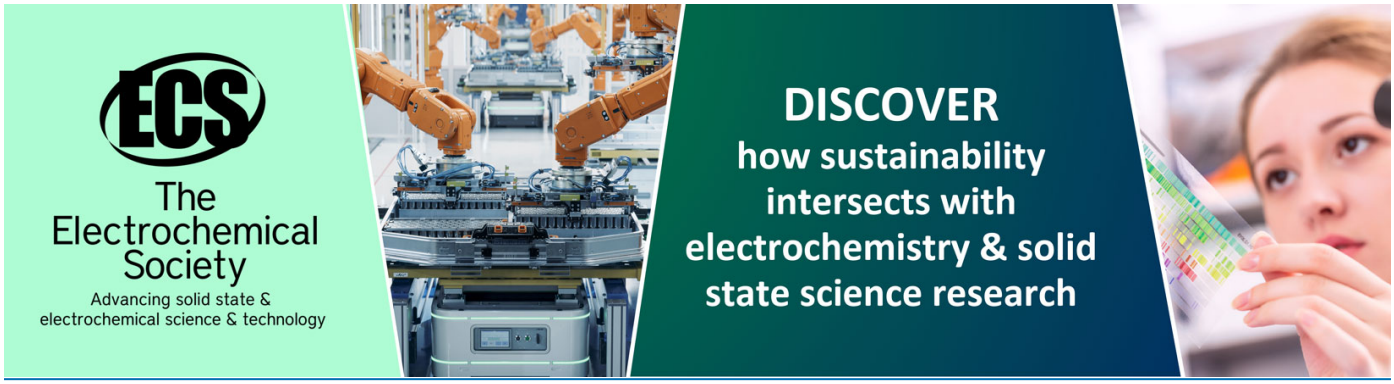
View the article online for updates and enhancements.

You may also like

- Poly(*D*, *L*-lactide-co-glycolide) nanoparticles as delivery agents for photodynamic therapy: enhancing singlet oxygen release and phototoxicity by surface PEG coating
Ester Boix-Garriga, Pilar Acedo, Ana Casadó et al.

- Oral pentamidine-loaded poly(d,l-lactic-co-glycolic) acid nanoparticles: an alternative approach for leishmaniasis treatment
Isabela Viol Valle, Monique Etnea Machado, Cristina da Costa Bernardes Araújo et al.

- Multilayer thin films of Zinc (II) Phthalocyanine loaded Poly(D, L-lactide-co-glycolide) nanocapsules by layer-by-layer self assembly
Yonca Belce and Fevzi Ç Cebeci



This content was downloaded from IP address 193.140.1.200 on 20/05/2024 at 21:00

OPEN ACCESS
IOP Publishing
Nanotechnology
Nanotechnology **35** (2024) 305602 (16pp)
https://doi.org/10.1088/1361-6528/ad403e

Synthesis of novel coumarin-triazole hybrids and first evaluation of the 4-phenyl substituted hybrid loaded PLGA nanoparticles delivery system to the anticancer activity

Busra Arvas[1], Burcu Ucar[2], Tayfun Acar[3], Hanife Sevgi Varli[4,5], Melih Besir Arvas[6], Feray Aydogan[1] and Cigdem Yolacan[1]

[1] Department of Chemistry, Faculty of Arts & Science, Yildiz Technical University, Istanbul, Turkey
[2] Department of Biomedical Engineering, Faculty of Engineering and Architecture, Istanbul Arel University, Istanbul, Turkey
[3] Department of Bioengineering, Faculty of Chemical and Metallurgical Engineering, Yildiz Technical University, Istanbul, Turkey
[4] Science and Technology Application and Research Center, Yildiz Technical University, Istanbul, Turkey
[5] Department of Molecular Biology and Genetics, Faculty of Arts & Science, Yildiz Technical University, Istanbul, Turkey
[6] Department of Chemistry, Faculty of Science, Istanbul University, Istanbul, Turkey

E-mail: cigdemyolacan@hotmail.com

Received 14 October 2023, revised 31 March 2024
Accepted for publication 18 April 2024
Published 7 May 2024

Abstract

Despite the discovery of many chemotherapeutic drugs that prevent uncontrolled cell division processes in the last century, many studies are still being carried out to develop drugs with higher anticancer efficacy and lower level of side effects. Herein, we designed, synthesized, and characterized six novel coumarin-triazole hybrids, and evaluated for anticancer activity of the one with the highest potential against the breast cancer cell line, MCF-7 and human cervical cancer cell line, human cervical adenocarcinoma (HeLa). Compound **21** which was the coumarin derivative including phenyl substituent with the lowest IC50 value displayed the highest cytotoxicity against the studied cancer cell line. Furthermore, the potential use of poly (lactic-co-glycolic acid) nanoparticles (PLGA NPs) prepared by the emulsifying solvent evaporation method as a platform for a drug delivery system was studied on a selected coumarin derivative **21**. This coumarin derivative-loaded PLGA NPs were produced with an average size of 225.90 $\pm$ 2.96 nm, -16.90 ± 0.85 mV zeta potential, and 4.12 $\pm$ 0.90% drug loading capacity. The obtained **21**-loaded PLGA nanoparticles were analyzed spectroscopically and microscopically with FT-IR, UV–vis, and scanning electron microscopy as well as thermogravimetric analysis, Raman, and x-ray diffraction. The *in vitro* release of **21** from the nanoparticles exhibited a controlled release profile just over one month following a burst release in the initial six hours and in addition to this a total release ratio of %50 and %85 were obtained at pH 7.4 and 5.5, respectively. **21**-loaded PLGA nanoparticles displayed remarkably effective anticancer activity

Original content from this work may be used under the terms of the Creative Commons Attribution 4.0 licence. Any further distribution of this work must maintain attribution to the author(s) and the title of the work, journal citation and DOI.

© 2024 The Author(s). Published by IOP Publishing Ltd

than **21**. The IC50 values were determined as IC_{50} (**21**-loaded PLGA nanoparticles): 0.42 ± 0.01 mg ml^{-1} and IC_{50} (free **21** molecule): 5.74 ± 3.82 mg ml^{-1} against MCF-7 cells, and as IC_{50} (**21**-loaded PLGA nanoparticles): 0.77 ± 0.12 mg ml^{-1} and IC_{50} (free **21** molecule): 1.32 ± 0.31 mg ml^{-1} against HeLa cells after the incubation period of 24 h. Our findings indicated that triazole-substituted coumarins may be used as an anticancer agent by integrating them into a polymeric drug delivery system providing improved drug loading and effective controlled drug release.

Supplementary material for this article is available online

Keywords: coumarin, PLGA nanoparticles, controlled drug release, MCF-7, anticancer activity, HeLa

1. Introduction

Coumarin and its derivatives constitue an important class of heterocyclic compounds with their benzopyran-2-one ring. They are useful compounds in various areas due to their important photophysical and biological activity properties. Especially, their biological activities such as anticoagulant, anticancer, antioxidant, antibacterial, antifungal, antimalarial make them good drug compounds and there are several coumarin derivatives in drug market [1–3]. These important biological activities are supplied by their active benzopyrone ring system with the ability to make hydrophobic, π–π and electrostatic interactions, hydrogen bonds besides van der Waals forces with receptors and a variety of enzymes [4].

The searches for compounds with specific activities turned the reseachers attention to hybrid molecules. The structure of a hybrid molecule can be created by the combination of two or more pharmacophores with different paths and activities to enhance the drug effect and balance the side effects. The pharmacophores in hybrid molecules may exhibit their own act on target or one of them can counterbalance the side effects of another parts. The hybrid compound may show properties from all pharmacophores with improved activity, affinity and selectivity, and they have the potential to broaden the biology spectrum and reduce side effects [5]. Especially, heterocyclic scaffold hybridization of coumarin compounds opens a new door for the novel drug development [6–13]. The easy functionalization of coumarin derivatives from different positions of ring carbons provides new hybrid molecules with promising activities. 1,2,3-triazole group containing molecules as therapeutic agents are known to show a wide range biological activity, such as antibiotic, antifungal and anticancer [4, 14, 15]. Coumarin and 1,2,3-trizole rings are important pharmacophore systems. Their combination in a hybrid molecule promise important biological activities [16–20]. Therefore, recently there has been a growing interest among researchers in the synthesis an evaluation of novel coumarin-triazole hybrid molecules.

Cancer is the second most deathful disease in the word. Early diagnosis and effective treatment can reduce the death ratio for most cancer types. There are some chemotherapeutic treatment methods using different drugs, but most of them have serious side effects [21]. So, the researces have been focused to develop effective drugs and drug systems without side effects. One of the recent approaches is drug delivery systems which are pharmaceutical formulations or devices. Drug delivery systems carry the bioactive molecules to the target organ through various biological barriers and release it in the targeted side of action. The encapsulation of drug molecule in nanoparticles is a promising approach to cancer treatment.

Polymeric nanoparticles with a size between 1 and 1000 nm are biomaterials that have a high drug loading capacity and provide controlled release of the loaded drug. The solvent evaporation method is the first method developed to prepare nanoparticles from a synthetic or natural polymers [22]. Many biocompatible polymers are used for production of nanoparticles, from natural polymers such as chitosan and alginate to synthetic polymers such as poly(lactic acid) (PLA), poly(glycolic acid) (PGA), and poly(lactide-co-glycolide) (PLGA) [23]. Since it is biocompatible and biodegradable (degradation to CO_2 and H_2O in the body) as well as approved by the FDA (Food and Drug Administration), PLGA is one of the most preferred polymers [23–28]. Also, there are various studies in which coumarin-derived compounds are loaded into PLGA nanoparticles [29, 30].

In this context, six novel coumarin-triazole hybrids (**16–21**, figure 1) were designed and chemically synthesized. The cytotoxic activities of the molecules whose structures were determined by FT-IR, TLC, ^{1}H and ^{13}C-NMR, and MS were evaluated by the MTT method and the best biocompatible compound **21** was loaded into the PLGA nanoparticles. The anticancer activity of the obtained **21**-loaded PLGA nanoparticles on MCF-7 cells was assessed.

2. Materials and methods

2.1. Materials and equipments

Acid terminated Poly(D,L-lactide-co-glycolic acid) (PLGA, lactide: glycolide molar ratio of 50:50, Mw = 38.000–54.000 Da) and poly(vinyl alcohol) (PVA, 98%–99% hydrolyzed, Mw = 31.000–50.000 Da) were purchased from Sigma Aldrich Chemicals (St. Louis) USA.

Commercial quality reagents were used for all experiments, and any further purification was not performed for reagent quality solvents. Millipore Milli-Q system (~18.2 MΩ cm) was used to obtain ultra-pure water. Silica gel 60 (40–63 μM) (Merck) was stationary phase for column

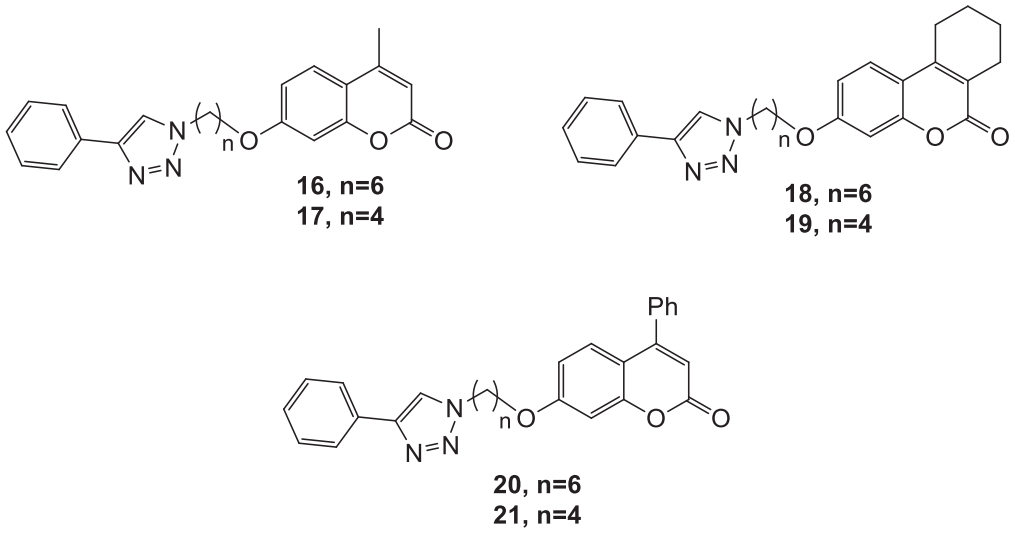


Figure 1. The structures of new coumarin-triazol hybrids.

chromatography and silica gel $60F_{254}$ coated aluminum sheets (Merck) were used for TLC.

The devices used to obtain spectral data were Perkin Elmer, Spectrum One FT-IR spectrometer and Bruker Tensor 27 spectrometer for IR spectra, Bruker Avance III 500 MHz spectrometer for NMR spectra, Agilent G6530B model TOF/Q-TOF Mass Spectrometer for LC-MS (Q-TOF) spectra. The chemical shifts δ were given in ppm according to TMS internal standard.

The MCF-7 human breast cancer, CCD1072 human fibroblast, HEK-293 (human embryonic kidney) and He-La (Human Cervical Adenocarcinoma) cell lines were provided from the Melisa Türkoğlu Laçin Regenerative Tissue and Cell Culture Laboratory (TURKEY) cell culture stocks.

2.2. Methods

2.2.1. Chemical synthesis. The synthesis of compounds **1–9** were carried out according to the literature procedure [31, 32]. Among the bromoalkyoxy compounds, only 3-(6-bromohexyloxy)−7,8,9,10-tetrahydro-6H-benzo[c]chromen-6-one (**6**) is not identified in the literature. The protocols for the synthesis of **6** and **10–21** according to the well-known methods were given in the following section. Spectroscopic data were used for characterization of all compounds. Original spectra of new compounds were given in the Supporting Information (figures S1–S36). The data of all known compounds were in accordance with literature data [31, 33, 34].

3-(6-Bromohexyloxy)-7,8,9,10-tetrahydro-6H-benzo[c] chromen-6-one (**6**)

The coumarin derivative **3** (1.0 mmol) and potassium carbonate (3.0 mmol) were stirred for 1 h at 55 °C in dry acetone, and then the dibromohexane (2.0 mmol) was added quite slowly. The mixture was refluxed for 24 h under nitrogen atmosphere. After cooling to room temperature, the solid was filtered and washed with acetone. The filtrate was concentrated under reduced pressure and purified by column chromatography using ethyl acetate/n-hexane as eluent to get the intermediates of **6**. White solid. Yield 70%. mp: 84 °C–85 °C. TLC $R_f = 0.39$ (EtOAc:hexane, 1:2, v/v). IR (ATR) ν 3067, 2936, 2884, 2862, 1704, 1606, 1500, 1468, 1449, 1392, 1262, 640 cm^{-1}. ^1H NMR (500 MHz, $CDCl_3$) δ1.52–1.54 (m, 4H, CH_2), 1.78–1.87 (m, 6H, CH_2), 1.88–1.94 (m, 2H, CH_2), 2.56 (bs, 2H, CH_2), 2.75 (bs, 2H, CH_2), 3.44 (t, 2H, $J = 6.5$ Hz, CH_2Br), 4.01 (t, 2H, $J = 6.5$ Hz, OCH_2), 6.79 (bd, 1H, $J = 2.5$ Hz, ArH), 6.82 (dd, 1H, $J = 9.0$ Hz, 2.5 Hz ArH), 7.44 (d, 1H, $J = 8.5$ Hz, ArH). ^{13}C NMR (125 MHz, $CDCl_3$) δ 21.41, 21.71, 23.84, 25.23, 25.25, 27.89, 28.87, 32.63, 33.74, 68.20, 101.11, 112.31, 113.66, 120.42, 124.08, 147.31, 153.51, 160.88, 162.20. LC-MS (ESI-QTOF): m/z calcd for $C_{19}H_{23}BrO_3$ $[M+H]^+$ 379.0903 found 379.0900.

General procedure for the synthesis of 7-azidoalkyloxy substituted coumarin derivatives (**10–15**)

A solution of sodium azide (NaN_3) (9 mmol) dissolved in distilled water (2 ml) was added to bromoalkyloxy coumarin derivatives (**4–9**) (3.0 mmol) dissolved in DMF (8 ml). The mixture was stirred at 80 °C for 24 h. The formed solution was cooled to room temperature then mixed with ice–water followed by extraction with ether. The ether evaportion was done after drying with $MgSO_4$. The obtained compounds were pure enough and used for the next step without any purification.

7-((6-Azidohexyl)oxy)-4-methyl-2H-chromen-2-one (**10**)

White solid. Yield 91%. mp: 40 °C–41 °C (Lit: 38 °C–40 °C [35, 36]). TLC $R_f = 0.28$ (EtOAc:hexane, 1:4, v/v). IR (ATR) ν 3073, 2969, 2933, 2859, 2106, 1719, 1609, 1562, 1463, 1389, 1104 cm^{-1}. ^1H NMR (500 MHz, $CDCl_3$) δ 1.44–1.55 (m, 4H, CH_2), 1.62–1.68 (m, 2H, CH_2), 1.81–1.87 (m, 2H, CH_2), 2.40 (s, 3H, CH_3), 3.30 (t, 2H, $J = 7.0$ Hz, CH_2N_3), 4.02 (t, 2H, $J = 6.5$ Hz, OCH_2), 6.13 (s, 1H, =CH), 6.80 (d, 1H, $J = 2.5$ Hz, ArH), 6.85 (dd, 1H, $J = 9.0$ Hz, 2.5 Hz, ArH), 7.49 (d, 1H, $J = 9.0$ Hz, ArH). ^{13}C NMR (125 MHz, $CDCl_3$) δ 18.67, 25.61, 26.47, 28.77, 28.86, 51.34, 68.31, 101.31, 111.85, 112.63, 113.46, 125.48, 152.56, 155.28, 161.34, 162.09. LC-MS (ESI-QTOF): m/z calcd for $C_{16}H_{19}N_3O_3$ $[M+H]^+$ 302.1460 found 302.1481.

7-(4-Azidobutoxy)-4-methyl-2H-chromen-2-one (**11**)

White solid (Lit. Cream solid, [35]). Yield 87%. mp: 64 °C–65 °C. TLC R_f = 0.46 (EtOAc:hexane, 1:4, v/v). IR (ATR) ν 3076, 2942, 2874, 2092, 1713, 1609, 1556, 1470, 1386, 1199 cm^{-1}. ^1H NMR (500 MHz, $CDCl_3$) δ 1.78–1.84 (m, 2H, CH_2), 1.89–1.95 (m, 2H, CH_2), 2.40 (s, 3H, CH_3), 3.39 (t, 2H, J = 6.5 Hz, CH_2N_3), 4.06 (t, 2H, J = 6.5 Hz, OCH_2), 6.14 (s, 1H, =CH), 6.80 (d, 1H, J = 2.5 Hz, ArH), 6.86 (dd, 1H, J = 9.0 Hz, 2.5 Hz, ArH), 7.50 (d, 1H, J =9.0 Hz, ArH). ^{13}C NMR (125 MHz, $CDCl_3$) δ 18.67, 25.66, 26.29, 51.11, 67.77, 101.33, 111.97, 112.58, 113.61, 125.55, 152.56, 155.26, 161.30, 161.88. LC-MS (ESI-QTOF): m/z calcd for $C_{14}H_{15}N_3O_3$ $[M+H]^+$ 274.1200 found 274.1164.

3-((6-Azidohexyl)oxy)-7,8,9,10-tetrahydro-6H-benzo[c]chromen-6-one (**12**)

Colorless viscous oil. Yield 90%. TLC R_f = 0.36 (EtOAc:hexane, 1:4, v/v). IR (ATR) ν 3089, 3067, 2943, 2862, 2093, 1697, 1606, 1568, 1469, 1429, 1391, 1260 cm^{-1}. ^1H NMR (500 MHz, $CDCl_3$) δ 1.45–1.56 (m, 4H, CH_2), 1.62–1.68 (m, 2H, CH_2), 1.78–1.88 (m, 6H, CH_2), 2.56 (m, 2H, CH_2), 2.75 (m, 2H, CH_2), 3.30 (t, 2H, J = 6.5 Hz, CH_2N_3), 4.01 (t, 2H, J = 6.5 Hz, OCH_2), 6.79 (d, 1H, J = 2.5 Hz, ArH), 6.83 (dd, 1H, J = 9.0 Hz, 2.5 Hz, ArH), 7.45 (d, 1H, J = 9.0 Hz, ArH). ^{13}C NMR (125 MHz, $CDCl_3$) δ 21.42, 21.73, 23.85, 25.25, 25.65, 26.50, 28.74, 28.92, 51.32, 68.20, 100.96, 112.43, 113.69, 120.47, 124.13, 147.31, 153.54, 160.09, 162.22. LC-MS (ESI-QTOF): m/z calcd for $C_{19}H_{23}N_3O_3$ $[M+NH_4]^+$ 359.2100 found 359.2082.

3-(4-Azidobutoxy)-7,8,9,10-tetrahydro-6H-benzo[c]chromen-6-one (**13**)

Beige solid. Yield 75%. mp: 88 °C–89 °C. TLC R_f = 0.32 (EtOAc:hexane, 1:1, v/v). IR (ATR) ν 3094, 3068, 2942, 2886, 2083, 1698, 1614, 1562, 1480, 1462, 1387, 1292 cm^{-1}. ^1H NMR (500 MHz, $CDCl_3$) δ 1.79–1.86 (m, 6H, CH_2), 1.89–1.94 (m, 2H, CH_2), 2.57 (t, 2H, J = 6.0 Hz, CH_2), 2.76 (t, 2H, J = 6.0 Hz, CH_2), 3.39 (t, 2H, J = 6.5 Hz, CH_2N_3), 4.05 (t, 2H, J = 6.0 Hz, OCH_2), 6.79 (bd, 1H, J = 2.5 Hz, ArH), 6.84 (dd, 1H, J = 9.0 Hz, 2.5 Hz, ArH), 7.47 (d, 1H, J = 9.0 Hz, ArH). ^{13}C NMR (125 MHz, $CDCl_3$) δ 21.39, 21.69, 23.84, 25.23, 25.69, 26.33, 51.13, 67.64, 101.10, 112.28, 113.82, 120.58, 124.14, 147.28, 153.50, 160.65, 162.18. LC-MS (ESI-QTOF): m/z calcd for $C_{17}H_{19}N_3O_3$ $[M+H]^+$ 314.1505 found 314.1500.

7-((6-Azidohexyl)oxy)-4-phenyl-2H-chromen-2-one (**14**)

Colorless viscous oil. Yield 86%. TLC R_f = 0.4 (EtOAc:hexane, 1:4, v/v). IR (ATR) ν 3075, 3054, 2944, 2914, 2865, 2085, 1714, 1600, 1549, 1491, 1422, 1374, 1266 cm^{-1}. ^1H NMR (500 MHz, $CDCl_3$) δ 1.45–1.56 (m, 4H, CH_2), 1.62–1.68 (m, 2H, CH_2), 1.82–1.87 (m, 2H, CH_2), 3.30 (t, 2H, J = 6.5 Hz, CH_2N_3), 4.04 (t, 2H, J = 6.5 Hz, OCH_2), 6.22 (s, 1H, =CH), 6.79 (dd, 1H, J = 9.0 Hz, 2.5 Hz, ArH), 6.88 (d, 1H, J = 2.5 Hz, ArH), 7.38 (d, 1H, J = 8.5 Hz, ArH), 7.43–7.45 (m, 2H, ArH), 7.50–7.53 (m, 3H, ArH). ^{13}C NMR (125 MHz, $CDCl_3$) δ 25.62, 26.49, 28.79, 28.86, 51.36, 68.39, 101.57, 111.79, 112.42, 112.69, 127.96, 128.39, 128.83, 129.58, 135.63, 155.85, 156.03, 161.28, 162.28. LC-MS (ESI-QTOF): m/z calcd for $C_{21}H_{21}N_3O_3$ $[M+H]^+$ 364.1616 found 364.1696.

7-(4-Azidobutoxy)-4-phenyl-2H-chromen-2-one (**15**)

Colorless solid. Yield 86%. mp: 60 °C–61 °C. TLC R_f = 0.89 (EtOAc:hexane, 1:1, v/v). IR (ATR) ν 3062, 2930, 2870, 2095, 1720, 1667, 1605, 1493, 1406, 1374, 1258 cm^{-1}. ^1H NMR (500 MHz, $CDCl_3$) δ 1.79–1.84 (m, 2H, CH_2), 1.90–1.96 (m, 2H, CH_2), 3.39 (t, 2H, J = 6.5 Hz, CH_2N_3), 4.08 (t, 2H, J = 6.0 Hz, OCH_2), 6.23 (s, 1H, =CH), 6.79 (dd, 1H, J = 9.0 Hz, 2.5 Hz ArH), 6.88 (d, 1H, J = 2.5 Hz, ArH), 7.39 (d, 1H, J = 8.5 Hz, ArH), 7.43–7.46 (m, 2H, ArH), 7.50–7.53 (m, 3H, ArH). ^{13}C NMR (125 MHz, $CDCl_3$) δ 25.66, 26.28, 51.11, 67.83, 101.57, 111.88, 112.63, 128.02, 128.38, 128.83, 129.60, 135.56, 155.83, 155.98, 161.25, 162.03. LC-MS (ESI-QTOF): m/z calcd for $C_{19}H_{17}N_3O_3$ $[M+H]^+$ 336.1300 found 336.1320.

General procedure for the synthesis of coumarin-triazole hydrids (16–21)

Azidoalkyloxy compound (0.138 mmol), phenylacetylene (0.16 mmol) and CuI (0.41 mmol) were mixed in tetrahydrofurane (5 ml) for 48 h at room temperature. Then, the mixture was filtered over celite. After the solvent evaporation, the purification of the crude product was acomplished by column chromatograpy. The elution solvent was ethyl acetate/hexane mixture.

4-Methyl-7-((6-(4-phenyl-1H-1,2,3-triazol-1-yl)hexyl)oxy)-2H-chromen-2-one (**16**)

Beige solid. Yield 86%. mp: 114 °C–115 °C. TLC R_f = 0.31 (EtOAc:hexane, 1:1, v/v). IR (ATR) ν 3075, 2941, 2863, 2854, 1722, 1605, 1558, 1466, 1450, 1428, 1262, 1070 cm^{-1}. ^1H NMR (500 MHz, $CDCl_3$) δ 1.42–1.48 (m, 2H, CH_2), 1.53–1.59 (m, 2H, CH_2), 1.79–1.85 (m, 2H, CH_2), 1.98–2.04 (m, 2H, CH_2), 2.38 (s, 3H, CH_3), 4.00 (t, 2H, J = 6.5 Hz, OCH_2), 4.43 (t, 2H, J = 7.0 Hz, NCH_2), 6.12 (s, 1H, =CH), 6.77 (bd, 1H, J = 2.5 Hz, ArH), 6.82 (dd, 1H, J = 8.5 Hz, 2.5 Hz, ArH), 7.32–7.35 (m, 1H, ArH), 7.41–7.47 (m, 3H, ArH), 7.76 (bs, 1H, ArH), 7.83 (bd, 2H, J = 7.0 Hz, ArH). ^{13}C NMR (125 MHz, $CDCl_3$) δ 18.67, 25.52, 26.21, 28.73, 30.24, 50.26, 68.20, 101.32, 111.86, 112.58, 113.49, 119.41, 125.51, 125.66, 128.11, 128.82, 130.63, 147.78, 152.58, 155.25, 161,33, 162.02. LC-MS (ESI-QTOF): m/z calcd for $C_{24}H_{25}N_3O_3$ $[M+H]^+$ 404.1929, found 404.1969.

4-Methyl-7-(4-(4-phenyl-1H-1,2,3-triazol-1-yl)butoxy)-2H-chromen-2-one (**17**)

Off-white solid. Yield 60%. mp: 116 °C–117 °C. TLC R_f = 0.39 (EtOAc:hexane, 2:1, v/v). IR (ATR) ν 3029, 2956, 2922, 2875, 1712, 1608, 1556, 1464, 1450, 1424, 1266, 1072 cm^{-1}. ^1H NMR (500 MHz, $CDCl_3$) δ 1.86–1.92 (m, 2H, CH_2), 2.16–2.22 (m, 2H, CH_2), 2.38 (s, 3H, CH_3), 4.04 (t, 2H, J = 6.0 Hz, NCH_2), 4.51 (t, 2H, J = 6.0 Hz, OCH_2), 6.11 (s, 1H, =CH), 6.77 (bd, 1H, J = 2.5 Hz, ArH), 6.82 (dd, 1H, J = 9.0 Hz, 2.5 Hz, ArH), 7.31–7.34 (m, 1H, ArH), 7.42 (t, 2H, J = 7.5 Hz, ArH), 7.47 (d, 1H, J = 9.0 Hz, ArH), 7.80 (s, 1H, ArH), 7.81–7.83 (m, 2H, ArH). ^{13}C NMR (125 MHz, $CDCl_3$) δ 18.65, 26.05, 27.08, 49.98, 67.42, 101.45, 112.03, 112.35, 113.71, 119.51, 125.62, 125.65, 128.17, 128.83, 130.55, 147.91, 152.22, 152.52, 161,23, 161.69. LC-MS (ESI-QTOF): m/z calcd for $C_{22}H_{21}N_3O_3$ $[M+H]^+$ 376.4300, found 376.1576.

3-((6-(4-Phenyl-1H-1,2,3-triazol-1-yl)hexyl)oxy)-7,8,9,10-tetrahydro-6H-benzo[c]chromen-6-one (**18**)

Beige solid. Yield 80%. mp: 140 °C–141 °C. TLC R_f = 0.16 (EtOAc:hexane, 1:2, v/v). IR (ATR) ν 3128, 3096, 3028, 2940, 2856, 1703, 1606, 1509, 1447, 1386, 1301, 1259, 1094 cm^{-1}. ^1H NMR (500 MHz, $CDCl_3$) δ 1.42–1.48 (m, 2H, CH_2), 1.52–1.59 (m, 2H, CH_2) 1.78–1.88 (m, 6H, CH_2) 1.98–2.05 (m, 2H, CH_2), 2.56 (t, 2H, J = 6.0 Hz, CH_2), 2.75 (t, 2H, J = 6.0 Hz, CH_2), 3.99 (t, 2H, J = 6.5 Hz, OCH_2) 4.44 (t, 2H, J = 7.0 Hz, N-CH_2), 6.77 (d, 1H, J = 2.5 Hz, ArH), 6.81 (dd, 1H, J = 9.0 Hz, 2.5 Hz, ArH), 7.32–7.35 (m, 1H, ArH), 7.41–7.44 (m, 3H, ArH), 7.76 (s, 1H, ArH), 7.82–7.84 (m, 2H, ArH). ^{13}C NMR (125 MHz, $CDCl_3$) δ 21.40, 21.70, 23.84, 25.23, 25.54, 26.23, 28.78, 30.27, 50.28, 68.07, 101.09, 112.29, 113.69, 119.40, 120.46, 124.12, 125.68, 128.12, 128.84, 130.63, 147.33, 147.79, 153.49, 160.79, 162.23. LC-MS (ESI-QTOF): m/z calcd for $C_{27}H_{29}N_3O_3$ $[M+H]^+$ 444.2242, found 444.2336.

3-(4-(4-Phenyl-1H-1,2,3-triazol-1-yl)butoxy)-7,8,9,10-tetrahydro-6H-benzo[c]chromen-6-one (**19**)

White solid. Yield 65%. mp: 149 °C–150 °C. TLC R_f = 0.56 (EtOAc:hexane, 2:1, v/v). IR (ATR) ν 3127, 3084, 2935, 2877, 1707, 1607, 1508, 1464, 1428, 1388, 1260, 1056. ^1H NMR (500 MHz, $CDCl_3$) δ 1.77–1.92 (m, 6H, CH_2), 2.16–2.22 (m, 2H, CH_2) 2.55 (bs, 2H, CH_2), 2.75 (bs, 2H, CH_2), 4.03 (t, 2H, J = 6.0 Hz, OCH_2) 4.51 (t, 2H, J = 6.0 Hz, N-CH_2), 6.76 (d, 1H, J = 2.5 Hz, ArH), 6.80 (dd, 1H, J = 9.0 Hz, 2.5 Hz, ArH), 7.31–7.34 (m, 1H, ArH), 7.40–7.43 (m, 3H, ArH), 7.79 (s, 1H, ArH), 7.81–7.83 (m, 2H, ArH). ^{13}C NMR (125 MHz, $CDCl_3$) δ 21.38, 21.68, 23.85, 25.20, 26.07, 27.12, 51.01, 67.30, 101.22, 112.03, 113.92, 119.48, 120.54, 124.20, 125.67, 128.13, 128.82, 130.56, 147.22, 147.90, 153.46, 160.45, 162.10. LC-MS (ESI-QTOF): m/z calcd for $C_{25}H_{25}N_3O_3$ $[M+H]^+$ 416.1974, found 416.1963.

4-Phenyl-7-((6-(4-phenyl-1H-1,2,3-triazol-1-yl)hexyl) oxy)-2H-chromen-2-one (**20**)

Colorless viscous oil. Yield 77%. TLC R_f = 0.27 (EtOAc:hexane, 1:2, v/v). IR (ATR) ν 3131, 3061, 2934, 2858, 1715, 1604, 1548, 1483, 1430, 1373, 1275, 1117 cm^{-1}. ^1H NMR (500 MHz, $CDCl_3$) δ 1.42–1.48 (m, 2H, CH_2), 1.53–1.60 (m, 2H, CH_2), 1.80–1.86 (m, 2H, CH_2), 1.99–2.05 (m, 2H, CH_2), 4.03 (t, 2H, J = 6.5 Hz, OCH_2), 4.44 (t, 2H, J = 7.0 Hz, N-CH_2), 6.21 (s, 1H, =CH), 6.77 (dd, 1H, J = 9.0 Hz, 2.5 Hz, ArH), 6.87 (d, 1H, J = 2.5 Hz, ArH), 7.32–7.37 (m, 2H, ArH), 7.41–7.44 (m, 4H, ArH), 7.51–7.54 (m, 3H, ArH), 7.76 (s, 1H, ArH),7.83 (bd, 2H, J = 7.0 Hz, ArH). ^{13}C NMR (125 MHz, $CDCl_3$) δ 25.52, 26.22, 28.74, 30.26, 50.26, 68.27, 101.56, 111.80, 112.44, 112.65, 119.39, 125.68, 127.98, 128.13, 128.38, 128.82, 128.84, 129.57, 130.64, 135.59, 147.82, 155.84, 156.00, 161.28, 162.19. LC-MS (ESI-QTOF): m/z calcd for $C_{29}H_{27}N_3O_3$ $[M+H]^+$ 466.2086, found 466.2206.

4-Phenyl-7-(4-(4-phenyl-1H-1,2,3-triazol-1-yl)butoxy)-2H-chromen-2-one (**21**)

White solid. Yield 68%. mp: 121 °C–122 °C. TLC R_f = 0.62 (EtOAc:petroleum benzine, 4:1, v/v). IR (ATR) ν 3120, 3069, 2965, 2949, 2873, 1716, 1603, 1552, 1471, 1426 1374, 1206, 1114 cm^{-1}. ^1H NMR (500 MHz, $CDCl_3$) δ 1.87–1.93 (m, 2H, CH_2), 2.17–2.23 (m, 2H, CH_2), 4.06 (t, 2H, J = 6.5 Hz, N-CH_2), 4.52 (t, 2H, J = 6.5 Hz OCH_2), 6.21 (s, 1H, =CH), 6.76 (dd, 1H, J = 9.0 Hz, 2.5 Hz, ArH), 6.86 (d, 1H, J = 2.5 Hz, ArH), 7.31–7.37 (m, 2H, ArH), 7.40–7.43 (m, 4H, ArH), 7.50–7.53 (m, 3H, ArH), 7.80 (s, 1H, ArH), 7.81–7.83 (m, 2H ArH) ^{13}C NMR (125 MHz, $CDCl_3$) δ 26.06, 27.08, 49.98, 67.48, 101.69, 111.96, 112.39, 112.66, 119.48, 125.67, 128.08, 128.18, 128.37, 128.84, 129.61, 130.55, 135.52, 147.93, 155.77, 155.95, 161.17, 161.84. LC-MS (ESI-QTOF): m/z calcd for $C_{27}H_{23}N_3O_3$ $[M+H]^+$ 438.1818, found 438.1758.

2.2.2. Preparation of the PLGA NPs. PLGA nanoparticles were prepared by the single emulsion solvent evaporation process according to our previous study with minor modifications [37]. Firstly, **21** and PLGA were dissolved in 750 μl and 2.5 ml DCM, respectively, and slightly vortexed. Then they were mixed each other. While the obtained solution was added dropwise into 4 ml of 3% (w/v) PVA in an ice bath, sonication was applied by using a probe sonicator (power of 80%, Bandelin Sonopuls, Germany) for 90 s. The formed single emulsion system was diluted in 35 ml of 0.1% (w/v) PVA solution. The obtained NPs were collected by centrifugation at 9000 rpm for 30 min (Nuve, NF 800R) and washed three times with ultrapure water using centrifugation at 9000 rpm for 20 min. Then, the NPs were lyophilized and storage −40 °C. The reaction yield (RY) of NPs was calculated using equation (1):

$$\mathrm{RY}(\%) = \frac{\text{Total amount of lyophilized NPs(mg)}}{\text{Amount of all excipients used in the formulation(mg)}} \times 100. \quad (1)$$

In order to calculate encapsulation efficiency (EE), and drug loading (DL) of NPs direct method was applied and equations (2) and (3) were used. For this purpose, 10 mg of solid, powder NPs was dissolved in 3 ml of DCM, vortexed, and shaken in an incubator (ES-20, Orbital Shaker, Biosan) at 180 rpm for one hour. All organic solvent was evaporated and the obtained solid was redispersed with water: ethanol (4:1). Insoluble particles were precipitated by centrifugation at 6000 rpm for 15 min and the supernatant was separated. This process was repeated two times [38]. The quantitative analysis was carried out by using a Shimadzu LC-MS (liquid chromatography–mass spectrometry) system (model LC-ESI-MS 2010 EV). The column was a Shim-Pack MRC-ODS-C18 HPLC with column oven temperature of 25 °C. The mobile phase consisted of A (water, 0.1% (v/v) FA) and B (ACN, 0.1% (v/v) FA) was at a flow rate of 0.6 ml min^{-1}.

The following mobile phase gradient elution was applied: 0–5 min, 50% B; 5.01–15 min, 50%–80% B; 15.01–25 min, %80 B; 25.01–30 min, 80%–50%; 30.01–40 min, 50% B [39]. Concentration determination was performed using UV-PDA detection at 210 and 280 nm, and was based on a previously created calibration curve given in Supporting Information, figure S37 (LC-MS calibration curve of the **21** coumarin derivative) (R^2:

0.9996, LOD: 2.45 μg ml^{-1}, LOQ: 7.44 μg ml^{-1}).

$$\mathrm{EE}(\%) = \frac{\text{Amount of drug determined in the NPs(mg)}}{\text{Amount of initially added drug(mg)}} \times 100 \quad (2)$$

$$\mathrm{DL}(\%) = \frac{\text{Amount of drug determined in the NPs(mg)}}{\text{Total amount of lyophilized NPs(mg)}} \times 100. \quad (3)$$

5 mg of the powder NPs were dispersed in 2.5 ml PBS at pH 7.4 or MES at pH 5.5 buffers to evaluate the *in vitro* release profile of the **21** from the NPs. At predetermined time intervals, all supernatant was separated by centrifugation at 9000 rpm for 15 min. The release media was filtered with 0.45 μm regenerated cellulose (RC) filter, and subjected to the analysis described above using the same LC-MS method and an appropriate calibration curve.

2.2.3. Characterization of the PLGA NPs. The obtained NPs were characterized by Zetasizer, ultraviolet–visible spectroscopy (UV–vis), Fourier-transform infrared spectroscopy-attenuated total reflectance (FT-IR-ATR), x-ray diffraction (XRD), Raman spectroscopy, differential thermal analysis (DTA), thermogravimetric analysis (TGA), and scanning electron microscopy (SEM). The mean size distribution, polydispersity index (PDI), and zeta potential of the NPs were determined by using Zetasizer (Zetasizer Nano ZS, Malvern, UK). Samples were freshly prepared before use by adding aliquots of NPs to PBS (pH 7.2) to make a solution with a NPs concentration of 1 mg ml^{-1}. Samples were diluted to 1:30 for the analysis and injected into a disposable capillary cell DTS1070 (Malvern Instruments, MA). Measurements were performed at 25 °C ± 1 °C with a material refraction index of 1.33, and viscosity of 0.8872 cp. All measurements were done in triplicate. The FT-IR spectra were recorded on Thermo Scientific Nicolet iS10 in ATR mode in ranging from 600 to 4000 cm^{-1} with resolution of 4 cm^{-1} and 32 scans were used [40–42]. The crystalline and/or amorphous structure of the NPs were evaluated by XRD analyes. Powder XRD patterns of the NPs were analyzed at room temperature with PANalytical X'Pert PRO powder diffractometer. The XRD spectra were recorded between 5° and 60° (2θ). The chemical composition of the free **21** molecule, empty and **21**-loaded PLGA nanoparticles were studied by Raman spectroscopy (Perkin Elmer Raman Station 400F) using an excitation wavelength of 785 nm at 100 mW. Raman spectra were recorded by averaging three acquisitions of 3 s in the range 250–3200 cm^{-1}. The thermal features of the free **21** molecule, empty and **21**-loaded PLGA nanoparticles were measured using DTA and TGA (SII Nanotechnology-SII6000 Exstar TG/DTA 6300). Shortly, approximately 5 mg of each sample was placed on an aluminum pan under a nitrogen atmosphere. The thermograms were obtained at a temperature range of 30 °C–800 °C with a heating rate of 2 °C min^{-1} [43, 44].

PVA content of the **21**-loaded PLGA nanoparticles was calculated by a colorimetric method [45]. 10 mg of the NPs were dispersed in 2 ml of 0.5 M NaOH and stirred for 15 min at 60 °C. 900 μl of 1 N HCl was added to the mixture for the aim of neutralization and the final volume was completed to 5 ml with distilled water. Then, freshly prepared 3 ml of 0.65 M boric acid, 1 ml of I_2/KI and 1.5 ml of distilled water were added to the environment, respectively. The UV–vis analysis were performed at 690 nm and PVA content of the **21**-loaded PLGA nanoparticles was determined by using a calibration curve of the PVA ($R^2 > 0.99$) given in Supporting Information, figure S38 (UV–vis calibration curve of the PVA).

The surface morphology of the **21**-loaded PLGA nanoparticles was evaluated by SEM, Zeiss, EVO-LS 10 as previously described [40]. The complex was fixed on metal studs and then coated with gold under vacuum. SEM photomicrograph was taken at an acceleration voltage of 7 kV.

2.2.4. In vitro cell culture assay. In the cell culture experiments, human fibroblast L929 (CCD1072-SK), HEK-293 (human embryonic kidney), MCF-7 (human breast adenocarcinoma), and human cervical adenocarcinoma (HeLa) cell lines were used. DMEM cell culture medium was used for culture cells. Each medium was enriched by 10% fetal bovine serum (FBS) and %1 penicillin (1000 U ml^{-1})-streptomycin (1000 lg ml^{-1}) solution. Both healthy and cancer cell lines were incubated at 37 °C, in a humidified atmosphere of 5% CO_2 and 99.9% humidity. The cells were passaged enzymatically with 0.25% trypsin-1 mM EDTA and subculturing was done by briefly rinsed the cell layer with 0.25% (w/v) trypsin-0.53 mM EDTA solution to remove all traces of serum [24].

2.2.4.1. Cytotoxicity assay. We utilized the MTT assay to determine the cytotoxicity of molecules **1–3** and **16–21** on human fibroblast L929 (CCD1072-SK) and HEK-293 cell lines by following the approach of the literature [46]. Briefly, the cells (1×10^5 cells ml^{-1}) were implanted on 96-well plates and cultured overnight. Various concentrations ranging from 0.0001 to 1 mg ml^{-1} (0.1; 0.5; 1; 5; 50; 500 and 1000 μg ml^{-1}, $n = 4$) of the molecules **1–3** and **16–21** solved in serum-free DMEM-F12 medium were added onto cells and incubated the cells for 24 h period of time at 37 °C. For investigation of the cell sensitivity against the agent, 10 μl of MTT [3-(4, 5-dimethylthiazol-2-yl)−2, 5-diphenyl tetrazolium bromide] solution (10 mg ml^{-1}) was added into all wells. When the conversion of intracellular purple formazan crystals was detected under the microscope as an indicator of viability (4 h at 37 °C), these crystals were isolated from the medium containing MTT and dissolved in 100 μl of DMSO. As a final step, colorimetric density in well plates was measured by means of an ELISA reader (Thermo Scientific Multiskan GO Microplate, USA) at 570 nm for each well [24, 47]. DMSO which is well known cytotoxic activity agent was used as a positive control and DMEM + 10% FBS culture medium was used as negative control. The percentage

of the viable cells was calculated using the equation (4):

$$\%\text{cellviability} = 100 \times \frac{\text{sampleabsorbance}}{\text{negativecontrolabsorbance}} \quad (4)$$

2.2.4.2. Anticancer activity assay. The anticancer activities of the compounds **16–21** were evaluated by *in vitro* method using MTT assay against MCF-7 and HeLa. The MTT assay described before was performed by inoculating cultured MCF-7 and HeLa cells (the number of cells was 10^4 cells per well) [48]. The six compounds (**16–21**) were added to wells in a concentrations of 1 mg ml^{-1} in four replicate ($n = 4$) after 24 h of seeding in DMEM-F12 medium including 10% FBS. The cells were incubated for 24 h and 48 h periods of time. MTT reagent was added to wells and incubated for 4 h at 37 °C until intracellular purple formazan crystals are visible under the microscope. MTT reagent were removed and 100 μl of the DMSO was added to each well and mixed gently on an orbital shaker for one hour at room temperature. The absorbance was measured at 570 nm for each well on an absorbance plate reader and cell viability ratios were calculated. A positive control DMSO was used as a known cytotoxic activity agent [49].

2.2.5. Statistical analysis. Statistical analyzes of the results were carried out using MS Excel 2016 and OriginPro 9.0 programs. A p value less than 0.05 was considered to be significant. All experiments were repeated at the least three times. The obtained data were given as mean ± standard deviation.

3. Results and discussion

3.1. Chemistry

At the beginning of synthesis, three coumarin derivatives (**1–3**) were prepared by Pechmann condensation starting from resorcinol and β-ketoester in TFA under ultrasonic effect. Then, the alkylation of the coumarin derivatives (**1–3**) from C–7 was carried out with the dihaloalkane derivatives in acetone under nitrogen atmosphere to give compounds **4–9**. In the third part of our study, coumarin azide products (**10–15**) were prepared by S_N2 reaction of **4–9** and NaN_3 in DMF. In the last part of synthesis, the triazole-coumarin hybrid molecules (**16–21**) whose structures were given in figure 1 were obtained for the first time in the literature by the azide–alkyne 1, 3-dipolar cycloaddition reaction between azides (**10–15**) and phenylacetylene. The synthesis of all coumarin derivatives were summarized in scheme 1. The structures of all new compounds and coumarin-triazole derivatives were elucidated by IR, mass, ^{1}H and ^{13}C-NMR spectral data.

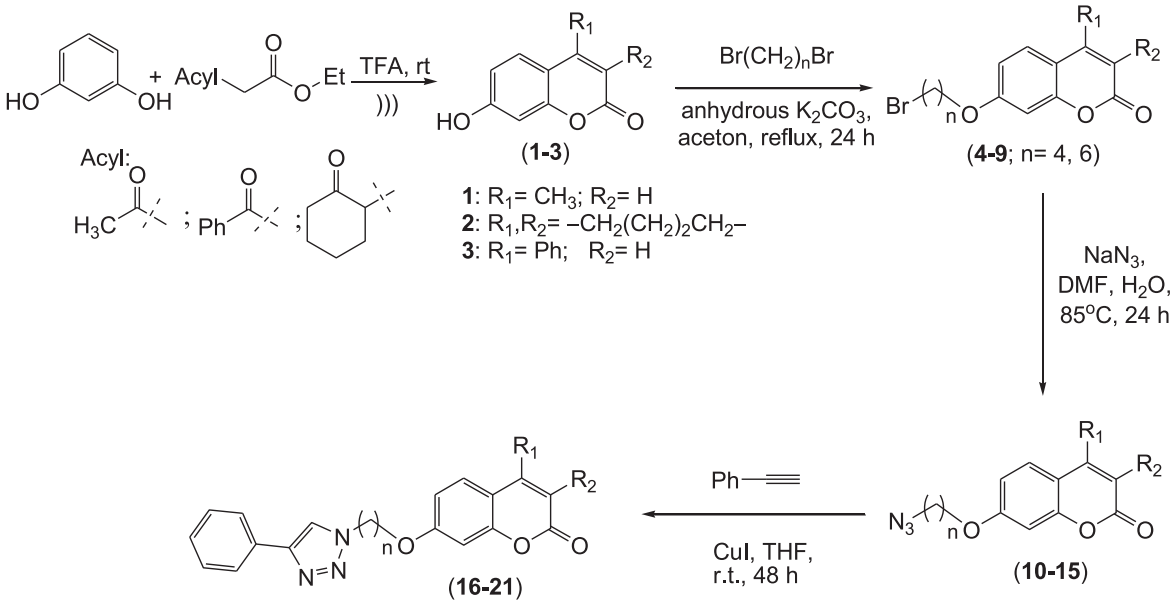
3.2. In vitro cytotoxicity assay

It has been previously emphasized that C4 and C7-substituted coumarin nucleus have great importance in the development of anti-cancer and anti-inflammatory drugs through their modifiable dual-site binding properties [50]. MTT assay was performed to analyze the cytotoxic potential of these coumarin derivatives in human fibroblast cell lines (CCD1072-SK). The viability of CCD1072-SK cells treated with **1–3**, **16–21** molecules prepared at various concentrations (0.1; 0.5; 1; 5; 50; 500 and 1000 μg ml^{-1}) decreased for each molecule with increasing concentration (**1**: 76%–21%; **2**: 81%–24%; **3**: 85%–22%, **16**: 111%–17%; **17**: 98%–27%; **18**: 110%–29%; **19**: 136%–26%; **20**: 121%–21%; **21**: 95%–18%) and also each molecule showed toxicity with different IC50 value (figure 2).

1,2,3-triazole derivatives have gained increasing popularity in recent years as an excellent building block for the discovery of potential anticancer agents [14, 51]. In this study, when the common hydroxyl of **1–3** molecules was replaced with 4-phenyl-1*H*-1,2,3-triazole of **16–21**, some differences, although not significant, were observed in the cytotoxicity values of the six molecules, **16–21**, compared to starting molecules **1–3**. With this result, it was thought that the three nitrogen atoms of the 1,2,3-triazole groups of the **16–21** molecules will may be exert an cytotoxic effect through different mechanisms by interacting with biological targets via hydrogen bonds [52]. The difference of substituents (methyl, cyclohexyl and phenyl) which are attached to the C4 carbon of the **17**, **19**, **21** (with $n = 4$C linker) and **16**, **18**, **20** (with $n = 6$C linker) molecules, may be affect the cytotoxicity levels as presented in the figure 2. The cytotoxicity values of **16–17**, **18–19** and **20–21** molecules with the alkyl linker with 6C and 4C atoms in the C7 carbon were also presented in the figure 2.

It was seen that decreasing of the carbon number in linker causes a significant increase in cytotoxicity values. In addition, it was observed that the methyl and cyclohexyl-linked molecules were more cytotoxic than the phenyl-linked ones when compared molecules **16**, **18**, and **20** substituted with same linker. This result supports that both of the linker and alkyl difference in the coumarin core directly affects the cellular behavior of the molecule.

However, with the decrease of the carbon number, there was observed a noticeable diminish in the solubility of molecule **19** in the experimental process so molecule **19** was considered inapplicable to *in vitro* analyzes and was excluded from the anticancer studies. Also, inconsistency of cellular analysis data due to high standard deviation for molecule **17** was determined. Considering these mentioned cons, the effect of substitutions at carbon C7 and C4 on the anticancer potential was evaluated with only molecules **16**, **18**, **20** and **21**. As a result of anticancer activity analyzes with MCF-7 cell line, the percent viability values for molecules **16**, **18**, **20** and **21** at the concentrations of 1 mg ml^{-1} were calculated as 80.2 ± 11.9%, 85.7 ± 2.6%, 84.3 ± 9.7% and 37.3 ± 2.6% (13.5 ± 0.1% for positive control) respectively (figure 3). It is seen in the graph that **16**, **18** and **20** molecules have very close to each other and low cytotoxicity values. In addition, it has been observed that when compared **20** and **21** containing phenyl substituents on C4, **21** with 4C linker was detected to have the highest anticancer effect as the optimum linker. In



Scheme 1. Schematic route of the synthesis.

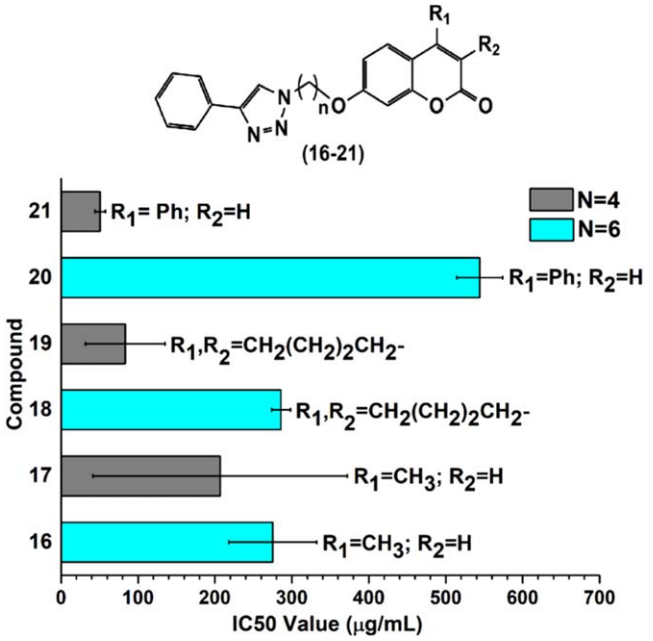


Figure 2. Experimentally observed IC50 values of the human fibroblast cells (CCD1072-SK) for coumarin-triazole hybrid molecules in 24 h period of time at 37 °C. Each value represents the mean ± SD ($n = 3$), M (μg ml^{-1}).

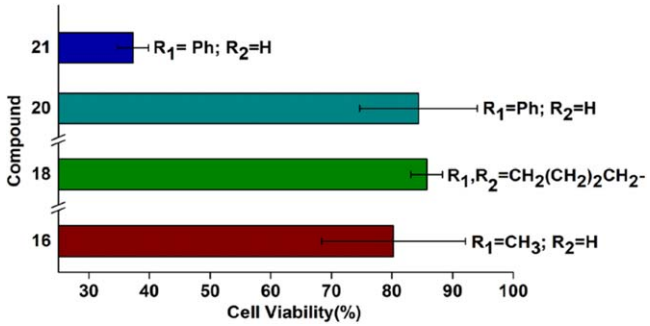


Figure 3. Percentage of MCF-7 cells viable following incubation with coumarin-triazole hybrid molecules (**16**, **18**, **20** and **21** at the concentrations of 1 mg ml^{-1}) relative to a control of untreated cells. Each bar represents the mean percentage survival and SD (where $n = 4$, four fields per repeat).

light of cell viability values obtained from the cell culture studies, molecule **21** was chosen for further studies. Primarily, a purity study was carried out utilizing HPLC for the **21** to make sure that the potential anticancer activity of the designed compound is not caused by possible impurities. The purity of **21** was found as 96% (Supporting Information, figure S39 HPLC chromatogram and purity information of **21**). To determine whether the low anti-cancer activities of the other three compounds (**16**, **18**, and **20**) were due to possible impurities, HPLC analysis was performed to present their impurities. The purity rates for molecules **16**, **18**, and **20** were 95% and above (Supporting Information, figures S40–42). Therefore, **21**, selected as the highest biocompatible molecule, was loaded into PLGA nanoparticles by a single emulsion solvent evaporation method to convert it into a functional material having the potential to treat breast carcinoma. It was aimed to diminish the existing toxicity and to increase the anticancer activity of the 21 molecule by developing an effective controlled release system.

3.3. Preparation of the 21-loaded PLGA nanoparticles

21 derivative which of 6 new coumarin derivatives obtained in this work with the lowest toxicity and the best biocompatible one in the human fibroblast cell line (CCD1072-SK), and the highest anticancer activity against MCF-7 cell line was incorporated into the PLGA nanoparticles by the solvent evaporation method. Thereby, it was aimed to minimize the existing toxicity of **21** and to enhance its anticancer activity with the controlled long release.

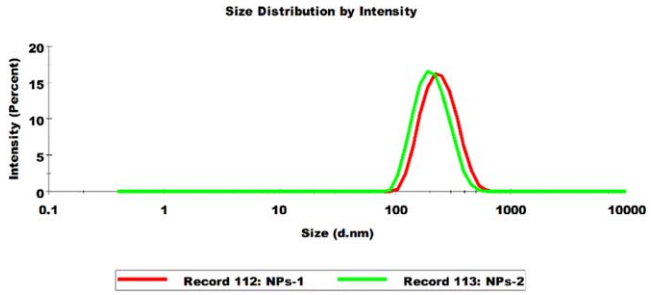


Figure 4. Size distribution by intensity of the NPs-1 (**21**-loaded PLGA nanoparticles) and NPs-2 (empty PLGA nanoparticles). For the measurements, NPs were freshly prepared at a concentration of 1 mg ml^{-1} and diluted with distilled water at a ratio of 1:30. The solutions were passed through neither 0.45 nor 0.22 μm filters.

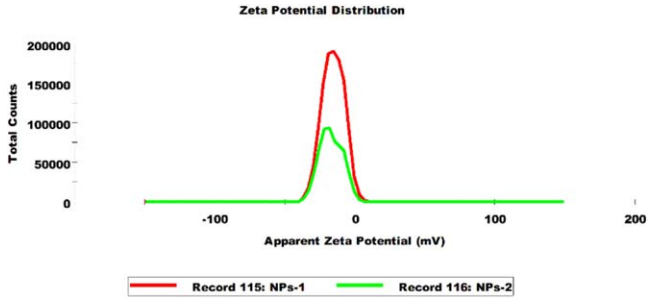


Figure 5. Zeta potential distribution of the NPs-1 (**21**-loaded PLGA nanoparticles) and NPs-2 (empty PLGA nanoparticles). For the measurements, NPs were freshly prepared at a concentration of 1 mg ml^{-1} and diluted with distilled water at a ratio of 1:30. The solutions were passed through neither 0.45 nor 0.22 μm filters.

RY, EE, and DL of the obtained **21**-loaded PLGA nanoparticles were found to be 66.35 ± 2.3%, 52.46 ± 3.8%, and 4.12 ± 0.9%, respectively. Our study exhibited not much difference in these data from previous studies [26, 53, 54]. The average particle sizes of empty and **21**-loaded PLGA nanoparticles were found to be 195.5 ± 1.411 nm and 225.9 ± 2.957 nm with PDI values of 0.102 ± 0.016 and 0.095 ± 0.023, respectively, which proved the homogenous distribution of the nanoparticles (figure 4). Some increase in average size occurred after the encapsulation process of **21** into PLGA NPs compare to empty NPs.

Furthermore, empty and **21**-loaded PLGA nanoparticles exhibited similar negative zeta potential of −16.9 ± 0.850 and −16.0 ± 0.115 mV thanks to the presence of PLGA terminal carboxylic groups and PVA residues on the surface (figure 5). This similarity also suggested to us that there was no significant drug adsorption on the NPs surface. At the same time, sufficiently negative zeta potential values provided prominent information about the stability of the nanoparticles. The zeta potential value of the **21**-loaded PLGA nanoparticles stored in lyophilized powder form at +4 °C for approximately 6 months was measured by the ELS technique. The zeta potential value of 21-loaded NPs measured under the same analysis conditions as in the initial measurements was found to be −15.0 ± 5.39 mV. This value proved to us that these nanoparticles were stable in long-term storage as well as there was no significant difference with the initial measurement. Additionally, for the full characterization of nanoparticles, it is also interesting to determine the ratio of the emulsifying agent used in the manufacturing of them in the produced nanoparticles. In this study, PVA, which is frequently used as an emulsifying agent in the production of PLGA nanoparticles, was preferred. Although excessive washing for removing PVA after the nanoparticles are produced, some of the PVA remains incorporated with the nanoparticles because it forms a mesh structure with the polymer at the interface. The PVA content of the **21**-loaded PLGA nanoparticles was found to be 3.87 ± 0.49% according to the colorimetric method and this value is convenient with the literature [55] (Supporting Information, figure S40, UV–vis spectrum of the **21**-loaded PLGA nanoparticles after the PVA concentration calculation method was applied).

FT-IR spectrum of the **21** showed some characteristic peaks (figure 6(a)). While 3120 and 3069 cm^{-1} corresponded to aromatic C–H stretches, 1716 and 1603 cm^{-1} referred to aromatic C=O and C=C groups, respectively. In addition, bands at 1471 and 1374 cm^{-1} represented aliphatic in-plane C–H bending, while 1206 cm^{-1} supported C–N oscillation, and 1114 cm^{-1} supported C–O tension. For PLGA, some peaks were examined in figure 6(a). The peaks between 2900 and 3000 cm^{-1} referred to C–H stretching of CH_3 groups, while the peak at 1748 cm^{-1} remarked carbonyl –C=O stretching and the other peaks between 1090 and 1171 cm^{-1} displayed the presence of C–O stretching. The spectra of empty and **21**-loaded PLGA nanoparticles exhibited completely the same characteristics. In addition, the absence of any specific peak belonging to the free **21** molecule in the spectrum of the **21**-loaded PLGA nanoparticles proved that the encapsulation process was carried out successfully and that the molecule did not adhere to the surface. This result was consistent with the results obtained in our previous studies [24, 27, 56].

The crystallization properties of the nanoparticles were examined by XRD. The XRD patterns of free **21** molecule, empty and **21**-loaded PLGA nanoparticles were presented in figure 6(b). There were sharp peaks in the 12–26 theta range, indicating that the **21** molecule is crystalline. In the spectra of empty and **21**-loaded PLGA nanoparticles, broadband in the 18.59 theta supporting the amorphous property of the PLGA were observed, similar to each other [57]. Thus, it was shown the **21** molecule was not found on the nanoparticle surface and successfully entrapped into the NPs.

The thermal behavior of the free **21** molecule, empty PLGA nanoparticles, and **21**-loaded PLGA nanoparticles was investigated by differential thermal analysis (DTA) and thermogravimetric analysis (TGA). Analysis of the free **21** molecule, (figure 7(a)) revealed one TGA step and three DTA peaks. The free **21** molecule had a single step TGA degradation point at 287 °C. The DTA steps were located at 121 °C, 386 °C and 662 °C. While the TGA thermogram of PLGA displayed a single phase of weight loss between 246 and 600 C, DTA revealed one step at 303 °C (figure 7(b)). Similar to empty nanoparticles, **21**-loaded PLGA nanoparticles also showed a single point weight loss, indicating that polymer and **21** molecule mixed but did not interact. In

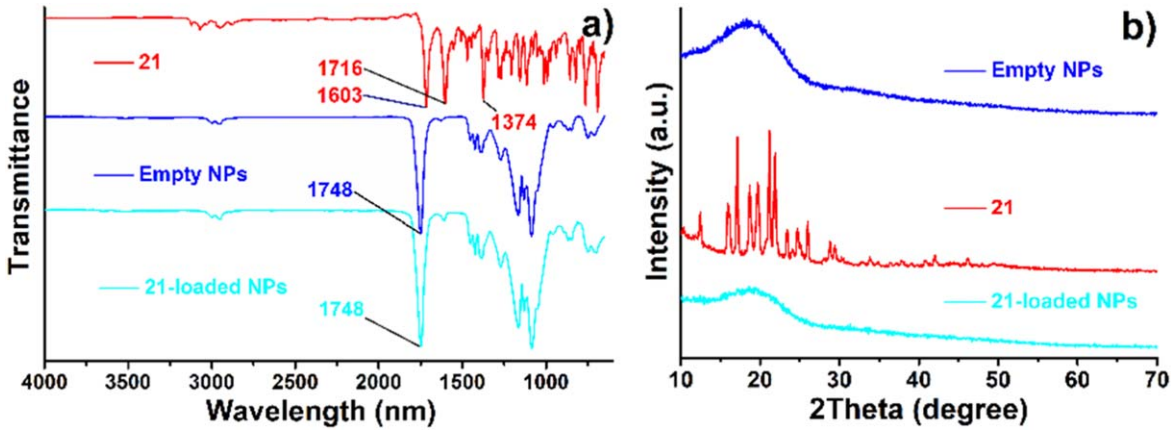


Figure 6. (a) The FT-IR spectra of empty and **21**-loaded PLGA nanoparticles comparatively with free **21** molecule (b) the XRD patterns of free **21** molecule, empty PLGA nanoparticles, and **21**-loaded PLGA nanoparticles.

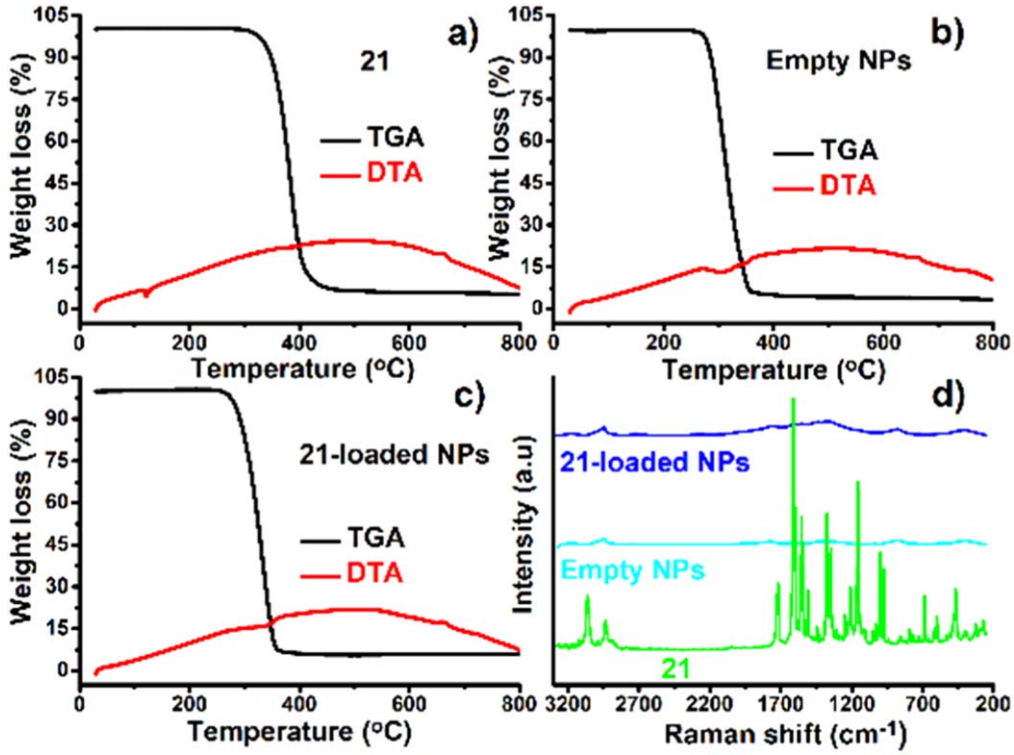


Figure 7. Thermal gravimetry and differential thermal analysis curves of the (a) free **21** molecule, (b) empty PLGA nanoparticles, (c) **21**-loaded PLGA nanoparticles, (d) Raman spectra of the free **21** molecule, empty PLGA nanoparticles, and **21**-loaded PLGA nanoparticles.

addition, the findings showed that the decomposition temperature reduces slightly with drug loading (figure 7(c)). The same result is well described in the literature [58]. TGA is also used to identify weight loss because of the volatilization of residual solvents in nanoparticles that take place around the boiling point of it [59]. Curiously, when both empty and **21**-loaded PLGA nanoparticles were analyzed by TGA, no considerable weight loss was monitored at the boiling point of DCM at 40 °C approving its absence as residual solvent.

In the Raman spectroscopy analysis, the representative peaks obtained from **21** and empty PLGA NPs were compared with the peaks for **21**-loaded PLGA nanoparticles (figure 7(d)). In the spectrum of empty PLGA NPs, peaks at 2752, 2946, and 3182 cm^{-1} refer to C−H stretching vibrations. One another band at 1770 cm^{-1} belongs to C=O bond stretching vibration while bands at 1114 cm^{-1} and 1036 cm^{-1} correspond to C–O stretching. Additionally, the C–H bend was noticed at 1436 cm^{-1}. When the Raman spectrum of the **21** was examined, it was determined that C–H bands at 3062, 2932 and 2890 cm^{-1}, C=O band at 1720 cm^{-1}, CH_3 band at 1378 cm^{-1}, C–C band at 1660 cm^{-1}. Besides the fact that the spectra of empty PLGA nanoparticles and **21**-loaded PLGA nanoparticles exhibited similar properties, no peaks of the **21**, the main peaks of which were given above, did not appear in

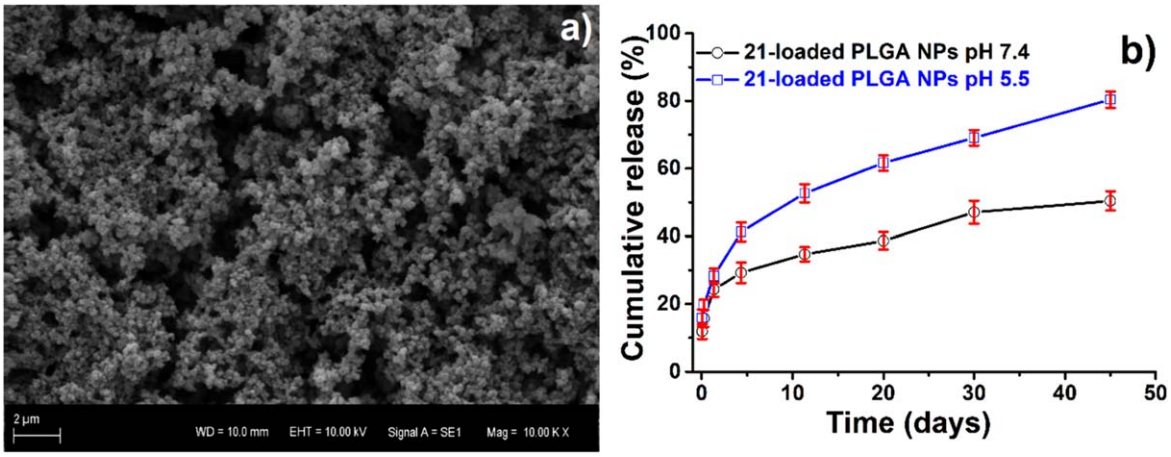


Figure 8. (a) SEM photograph of **21**-loaded PLGA nanoparticles produced by single emulsion solvent evaporation method (b) *in vitro* release profile of **21** from PLGA NPs in PBS buffer at pH 7.4 and in MES buffer at pH 5.5.

the spectra of the encapsulated PLGA nanoparticles, and this confirmed the encapsulation of **21** into PLGA nanoparticles with no surface adsorption.

SEM image showing the morphology of the **21**-loaded PLGA nanoparticles was presented in figure 8(a). In SEM imaging, parameters such as being able to determine the morphological distribution of the nanoparticles, being able to monitor the structural form of the nanoparticles, resolution of the images, and not deforming the samples during the analysis are important. We observed homogeneously dispersed and spherical nanoparticles supported by a high-resolution SEM image compatible with the Zetasizer measurement results.

Figure 8(b), represented the *in vitro* release profile of **21** from PLGA nanoparticles in two different buffered solutions at pH 5.5 and 7.4 at 37 °C. *In vitro* release behavior was evaluated for various time intervals (1, 6, 32 h; 4, 11, 20, 30, and 45 d). In the beginning, a typical initial burst release of **21** from the PLGA nanoparticles was seen for both release patterns and 15%–17% of the **21** was released from the nanoparticles in the first six hours. Burst release usually occurs when a certain amount of the drug encapsulated in a particle system is released into both the *in vitro* and *in vivo* release environment within a short period of 24–48 h. Even though this situation is attributed to different physical and chemical conditions, the primary mechanism of burst release in monolithic polymeric systems has not been utterly elucidated [60, 61]. The release of the active substance from PLGA nanoparticles occurs due to both diffusion and erosion. In addition, since PLGA is a polymer with the capacity to absorb water, polymeric degradation takes place both within the bulk and on the surface of the obtained nanoparticles. Since all these parameters interact with each other during the release of the active substance, their analysis becomes difficult. *In vitro* cumulative drug release patterns exhibit behavior in four different categories: monophasic, burst biphasic, delayed biphasic, and triphasic. The burst biphasic, termed 'burst release,' is typically characterized by rapid drug release upon initial exposure of PLGA nanoparticles to aqueous media, with the duration of this phase varying from several hours to 1–2 d [62]. Subsequently, it was assessed that **21** showed controlled release over a one-month period for both pH values. Following the initial burst release seen in the PLGA nanoparticles, a phase happens with a power law relationship between the cumulative amount of drug released and the time elapsed in this phase. In such a case, the zero-order release phase is observed, where the drug release rate becomes constant, meaning that the active material is released from the polymer depot via non-Fickian diffusion for a period of several days to weeks [62]. This constant release drew a profile that remained stable at the end of 45 d and continued to release at a low sustained rate which was undetectable by LC-MS. A similar kinetic pattern has been determined for other PLGA NPs [63]. The release profile of **21** from PLGA nanoparticles appears similar to coumarin C75 release from the same polymeric system found by Fernandes et al. where around 30% of the active ingredient was released until the first 24 h, followed by a sustained release which prolongs up to 7 d. Overall, while there was nearly 85% release of the drug at pH 5.5, the *in vitro* release is just about 50% at pH 7.4 for the same sample. It was evaluated that the parameters contributing to the *in vitro* release of **21** from nanoparticles were swelling of the PLGA polymer, pore diffusion, polymer erosion and degradation [57]. The fact that the release was notably higher under cancer microenvironment conditions at pH 5.5 can provide more valuable data for the anticancer cell study compared to pH 7.4.

3.4. In vitro anticancer activities

The *in vitro* cytotoxicity levels and anticancer activities of the three groups consisting of molecule **21**, **21**-loaded PLGA nanoparticles and empty PLGA NPs at five different concentrations were determined according to the survival rates of human fibroblast L929 cells, human embryonic kidney HEK-293 cells, (Supporting Information, figures S44–S45), human breast cancer MCF-7 cells, and HeLa cell lines by MTT analysis as well (figures 9–10). The negative control absorbance value was accepted as 100% viability for both tests. As shown in figures S44 and S45, **21**, **21**-loaded PLGA nanoparticles and empty PLGA NPs had almost no cytotoxicity

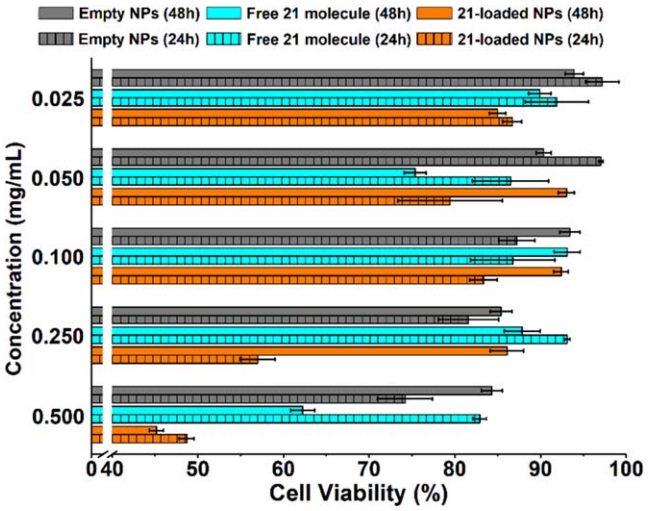


Figure 9. Dose response in MCF-7 cells treated with free **21** molecule, **21**-loaded PLGA nanoparticles, and empty NPs by MTT assay after 24 h and 48 h incubation time (all cell viability values represent the mean ± SD ($n = 5$), Apsis values; M (mg ml^{-1})).

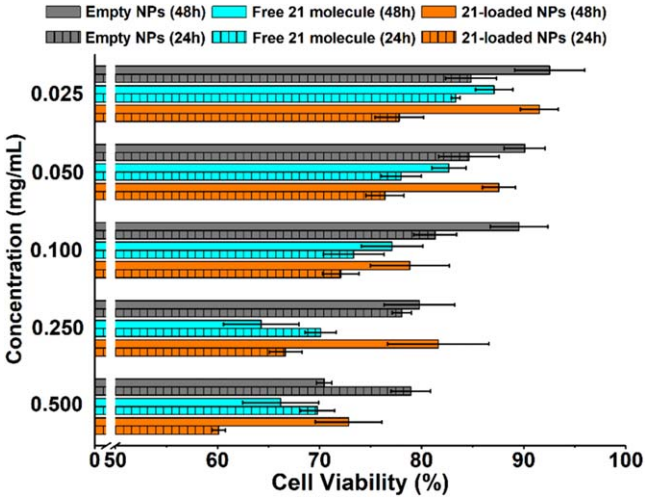


Figure 10. Dose response in MCF-7 cells treated with free **21** molecule, **21**-loaded PLGA nanoparticles, and empty NPs by MTT assay after 24 h and 48 h incubation time (all cell viability values of represent the mean ± SD ($n = 5$), Apsis values; M (mg ml^{-1})).

against human fibroblasts (CCD1072-SK) and HeLa cervical adenocarcinom cells. The viability of cells ranged between 70%–95% and 71%–94%, respectively.

With the encapsulation of molecule **21**, we observe an increase in cell viability (after incubation time of 24 h) against both MCF-7 breast cancer and HeLa cervical adenocarcinoma cells (figures 9–11). While an increase in cytotoxicity values indicating cell viability was observed from IC50$_{(\mathbf{21}\text{-loaded PLGA nanoparticles})}$: 0.77 ± 0.12 mg ml^{-1} to IC50$_{(\text{free } \mathbf{21} \text{ molecule})}$: 4.66 ± 3.36 mg ml^{-1} for HeLa cells, was observed from IC50$_{(\mathbf{21}\text{-loaded PLGA nanoparticles})}$: 0.42 ± 0.01 mg ml^{-1} to IC50$_{(\text{free } \mathbf{21} \text{ molecule})}$: 5.74 ± 3.82 mg ml^{-1} for MCF-7 cells (figure 11). This dramatic increase was evaluated as a result consistent with the burst release character resulting from the structure of the polymeric nanoparticle. The fact that about 20% of the total active ingredient release occurs during the first six hours (figure 8(b)) supports both the time-dependent and dose-dependent cytotoxic effects observed after incubation of 24 h (figures 9, 10). However, a series of cellular tests are needed to prove through which pathway the observed cytotoxic effect occurs. According to the results obtained in this study, it is clear that active molecule **21** acts at a sufficient dose and time to inhibit the proliferation of the tested cancer cells. However, when the IC50 graphs of the studied cancer cells are examined, the cytotoxicity values no increasing consistently with concentration and time may suggest that molecule **21** acts as a pro-apoptic agent on cancer cells. The proliferation of cancer cells, which reduce mitochondria permeability as a result of apoptosis, regardless of the applied dose, may result in increased cell viability. For this reason, despite the cumulative release in the second 24 h (figure 8(b)), cell viability may increase compared to the first 24 h. On the other hand, considering the hydrophobic character of the PLGA nanoparticles compared to the free molecule **21**, the delivery time and dose of the activated substance into the cell may differ and the duration of the cytotoxic effect may increase due to the increase in the exposure time to the active substance. In fact, as emphasized in the literature regarding coumarin derivatives, molecule **21** can suppress the growth and proliferation of cancer cells even at low doses and may not have a significant toxic effect on normal cells [64, 65]. This may be further evidence that coumarins are a promising class of anti-tumor drugs with high selectivity.

By the end of 2020, approximately 8 million women worldwide have been diagnosed with breast cancer, making it the most common and leading cause of death in women [66]. Different treatment methods and/or drugs that have been researched for many years aim not only to eliminate the disease but also to protect existing healthy tissues. There are many studies in literature on the structure–activity relationship of coumarin derivatives as anticancer drug candidates [11, 67–71]. However, the study examining the anticancer effect of synthetic coumarin-7 derivatives both to increase the drug-activity relationship and with biodegradable polymeric controlled release system is quite limited. When the activities of coumarin derivatives integrated with polymeric and other nanocarrier systems on MCF-7 breast cancer line are examined; the determined lowest IC50 value in which different coumarin extract types was calculated as 1.755 mg ml^{-1} [72]. In a separate study that treated breast cancer cell lines with zinc oxide nanostructures coated with ruthenium(III) complexes of synthetic coumarin derivatives, it was emphasized that ruthenium(III) complexes (IC50 $< 10\,\mu$g ml^{-1}) had a better value than the coated complex coated nanostructures (IC50 $< 80\,\mu$g ml^{-1}) [73]. In our study, IC50 values determined by encapsulating to the PLGA carrier system of synthetic coumarin-7 derivatives against MCF-7 breast cancer and HeLa cervical cancer cells were calculated as 0.42 ± 0.01 mg ml^{-1} and 0.77 ± 0.12 mg ml^{-1} respectively. Although the effect of polymeric controlled release system on cytotoxicity is already known, many synthetic coumarin molecules with different functional groups are difficult and limiting for *in vitro* cell studies due to solubility, hydrophobicity and high toxicity problems to healthy cells when

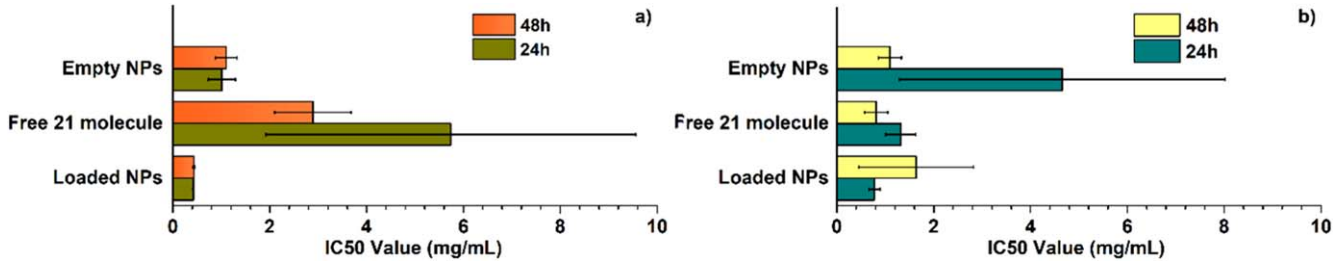


Figure 11. Calculated IC50 values of the **21**-loaded NPs, free **21** molecule and empty NPs against (a) MCF-7 and (b) HeLa cells after 24 and 48 h treatment (all values represent the mean ± SD ($n = 3$), IC50 (mg ml^{-1})).

compared to plant extract and protein/peptide structures. For this reason, we believe that our study will contribute significantly to the existing literature in terms of not only the unique molecules it contains, but also its combination with a delivery system and its *in vitro* evaluation. **21**-loaded PLGA nanoparticles can be given active targeting properties by conjugating them with peptides that have specific binding properties to the cancer cells of interest, thereby achieving a much higher level of anticancer activity. However, in cancer therapies, therapeutic agents are administered to patients in saline (0.9% NaCl solution). Therefore, evaluation of *in vitro* analyzes in this solution may strengthen the study.

4. Conclusion

Six new coumarin-triazole hybrids featuring different substituents at C4 position (methyl, phenyl or cyclohexyl) with two different chain linker lengths ($n = 4$, 6) were prepared and characterized by using ^{1}H NMR, ^{13}C NMR, and mass spectroscopy techniques. Since the relation of anticancer activity with cytotoxicity is known, first of all, a kind of pre-elimination was performed for all structures as a result of the cytotoxicity study. Even molecules that could not be applied to laboratory analysis procedures were eliminated. In this study, **21** was prominent as the most suitable molecule for the highest cytotoxicity against MCF-7. The superior properties of nanoparticles such as aggregation in leaky blood vessels of tumors and destroying tumors, minimizing damage to healthy organs, circulating in the bloodstream for a longer time, and optimizing the effective dose are known. Therefore, despite a certain level of *in vitro* anticancer activity of molecule **21**, the nanoparticle system was preferred for increasing its anticancer efficiency. The release profile, size, and production quality of the produced nanoparticles were evaluated and compared with the active substance itself in terms of its anticancer properties. On the whole, coumarin compounds can inhibit the growth, proliferation and metastasis of various tumor cells through various mechanisms (inhibition of carbonic anhydrase, PI3K/AKT/mTOR signaling pathway, microtubule polymerization, angiogenesis, monocarboxylate transporters, hypoxia inducible factor-1) acting on apoptosis proteins and inhibiting tumor multidrug resistance, ROS regulation, etc Coumarin derivatives have long been proven to be drug candidates acting as antitumor agents, with selective and effective cytotoxicity through various antitumor mechanisms. The failure to comprehensively study coumarin derivatives modified with different functional groups results in the limitation of *in vitro* and *in vivo* experiments to explore the relationship between these derivatives and their biological mechanisms and misunderstanding of drug pharmacokinetics and safety profile. The most well-known limitations can be listed as the fact that antitumor mechanisms have not been evaluated comprehensively, *in vitro* experiments are not supported by *in vivo* experiments in proving the *in vivo* antitumor potential and safety profile of newly discovered coumarin compounds, and finally, the newly discovered coumarin compounds are poorly soluble in water. Presented study was designed to overcome the limitation of *in vitro* studies due to the poor water solubility of coumarin compounds and the problem of low bioavailability. It involves increasing water solubility and bioavailability by modifying the functional groups of coumarin core, as well as increasing the biological performance of the molecule with a carrier system. We aimed to canalize the literature on the modification and delivery systems of coumarins by ensuring high selectivity, lower side effects and higher bioavailability. Due to the 2H-chromen-2-one ring (contributes to aromatic, planar and lipophilic structure), lactone group and heterocyclic conformation in the structure of coumarin enables interaction with different biological target proteins and forms strong polar bonds. Considering the results of cytotoxic activity, **21**-loaded PLGA nanoparticles (0.5 mg ml^{-1}) were determined as the most effective group with about 45% and 60% or higher survivals in MCF-7 cells and HeLa cells. In conclusion, in the study, the efficiency of molecule **21** selected among the novel six coumarin derivatives as potential anticancer drug candidates against breast and cervical adenocarcinom cells was extended with the integration to the polymeric nanosystem. We hope that this work can hereby chart a new avenue for the future optimization of candidate molecules with stronger anticancer properties.

Acknowledgments

This work was supported by Yildiz Technical University Scientific Research Foundation [project number FDK-2022-4971].

Data availability statement

The data cannot be made publicly available upon publication because they are not available in a format that is sufficiently accessible or reusable by other researchers. The data that support the findings of this study are available upon reasonable request from the authors.

Conflicts of interest

There are no conflicts to declare.

Ethical policy

In accordance with IOPP's Ethical Policy, all authors declare their consent to publication in the study involving identifiable human subjects (including cell or tissue donors).

Author contributions

BA, BU, TA, HSV and MBA carried out the experiments, BA, BU, TA, FA and CY contributed to conception, design and wrote the manuscript. All authors provided critical feedback and helped shape the research, analysis and manuscript.

ORCID iDs

Tayfun Acar https://orcid.org/0000-0001-5006-8167

References

[1] Bouhaoui A, Eddahmi M, Dib M, Khouili M, Aires A, Catto M and Bouissane L 2021 Synthesis and biological properties of coumarin derivatives. A review *ChemistrySelect* **6** 5848–70
[2] Hassan M Z, Osman H, Ali M A and Ahsan M J 2016 Therapeutic potential of coumarins as antiviral agents *Eur. J. Med. Chem.* **123** 236–55
[3] Ostrowska K 2020 Coumarin-piperazine derivatives as biologically active compounds *Saudi Pharm. J.* **28** 220–32
[4] Zhang L and Xu Z 2019 Coumarin-containing hybrids and their anticancer activities *Eur. J. Med. Chem.* **181** 111587
[5] Feng D, Zhang A, Yang Y and Yang P 2020 Coumarin-containing hybrids and their antibacterial activities *Arch. Pharm.* **353** 1900380
[6] Fan Y L, Ke X and Liu M 2018 Coumarin–triazole hybrids and their biological activities *J. Heterocycl. Chem.* **55** 791–802
[7] Husain A, Balushi K A, Akhtar M J and Khan S A 2021 Coumarin linked heterocyclic hybrids: a promising approach to develop multi target drugs for alzheimer's disease *J. Mol. Struct.* **1241** 130618
[8] Ibrar A, Shehzadi S A, Saeed F and Khan I 2018 Developing hybrid molecule therapeutics for diverse enzyme inhibitory action: active role of coumarin-based structural leads in drug discovery *Bioorg. Med. Chem.* **26** 3731–62
[9] Medina F G, Marrero J G, Macías-Alonso M, González M C, Córdova-Guerrero I, García A G T and Osegueda-Robles S 2015 Coumarin heterocyclic derivatives: chemical synthesis and biological activity *Nat. Prod. Rep.* **32** 1472–507
[10] Nouraie P, Moradi Dehaghi S and Foroumadi A 2019 Coumarin-1,2,3-triazole hybrid derivatives: green synthesis and DFT calculations *Synth. Commun.* **49** 386–94
[11] Rawat A and Reddy A V B 2022 Recent advances on anticancer activity of coumarin derivatives *Eur. J. Med. Chem. Rep.* **5** 100038
[12] Song X F, Fan J, Liu L, Liu X F and Gao F 2020 Coumarin derivatives with anticancer activities: an update *Arch. Pharm.* **353** 2000025
[13] Ye X-W, Zheng Y-C, Duan Y-C, Wang M-M, Yu B, Ren J-L, Ma J-L, Zhang E and Liu H-M 2014 Synthesis and biological evaluation of coumarin–1,2,3-triazole–dithiocarbamate hybrids as potent LSD1 inhibitors *MedChemComm* **5** 650–4
[14] Da Silva G D, Da Silva M G, Souza E M, Barison A, Simões S C, Varotti F P, Barbosa L A, Viana G H and Villar J A 2012 Design and synthesis of new chacones substituted with azide/triazole groups and analysis of their cytotoxicity towards HeLa cells *Molecules* **17** 10331–43
[15] Jabeen F, Shehzadi S A, Fatmi M Q, Shaheen S, Iqbal L, Afza N, Panda S S and Ansari F L 2016 Synthesis, *in vitro* and computational studies of 1, 4-disubstituted 1,2,3-triazoles as potential α-glucosidase inhibitors *Bioorg. Med. Chem. Lett.* **26** 1029–38
[16] El-Sayed W A, Alminderej F M, Mounier M M, Nossier E S, Saleh S M and Kassem A F 2022 Novel 1,2,3-triazole-coumarin hybrid glycosides and their tetrazolyl analogues: design, anticancer evaluation and molecular docking targeting EGFR, VEGFR-2 and CDK-2 *Molecules* **27** 2047
[17] Kraljević T G, Harej A, Sedić M, Pavelić S K, Stepanić V, Drenjančević D, Talapko J and Raić-Malić S 2016 Synthesis, *in vitro* anticancer and antibacterial activities and in silico studies of new 4-substituted 1,2,3-triazole–coumarin hybrids *Eur. J. Med. Chem.* **124** 794–808
[18] Najafi Z, Mahdavi M, Saeedi M, Karimpour-Razkenari E, Edraki N, Sharifzadeh M, Khanavi M and Akbarzadeh T 2019 Novel tacrine-coumarin hybrids linked to 1,2,3-triazole as anti-Alzheimer's compounds: *in vitro* and *in vivo* biological evaluation and docking study *Bioorg. Chem.* **83** 303–16
[19] Su Q, Xu B, Tian Z and Gong Z 2022 Design and development of novel 1,2,3-triazole chalcone derivatives as potential anti-osteosarcoma agents via inhibition of PI3K/Akt/mTOR signaling pathway *Acta Pharm.* **72** 389–402
[20] Vagish C B, Kumara K, Vivek H K, Bharath S, Lokanath N K and Kumar K A 2021 Coumarin-triazole hybrids: design, microwave-assisted synthesis, crystal and molecular structure, theoretical and computational studies and screening for their anticancer potentials against PC-3 and DU-145 *J. Mol. Struct.* **1230** 129899
[21] Weng K-G and Yuan Y-L 2017 Synthesis and evaluation of coumarin derivatives against human lung cancer cell lines *Braz. J. Medi. Biol. Res.* **50** e6455
[22] Zielińska A, Carreiró F, Oliveira A M, Neves A, Pires B, Venkatesh D N, Durazzo A, Lucarini M, Eder P and Silva A M 2020 Polymeric nanoparticles: production, characterization, toxicology and ecotoxicology *Molecules* **25** 3731
[23] Szczęch M and Szczepanowicz K 2020 Polymeric core–shell nanoparticles prepared by spontaneous emulsification solvent evaporation and functionalized by the layer-by-layer method *Nanomaterials* **10** 496
[24] Abamor E S, Allahverdiyev A, Tosyali O A, Bagirova M, Acar T, Mustafaeva Z and Derman S 2019 Evaluation of *in vitro* and *in vivo* immunostimulatory activities of poly

(lactic-co-glycolic acid) nanoparticles loaded with soluble and autoclaved Leishmania infantum antigens: a novel vaccine candidate against visceral leishmaniasis *Asian Pac. J. Tropical Med.* **12** 353–64

[25] Sarani M, Roostaee M, Adeli-Sardou M, Kalantar-Neyestanaki D, Mousavi S A A, Amanizadeh A, Barani M and Amirbeigi A 2024 Green synthesis of Ag and Cu-doped Bismuth oxide nanoparticles: revealing synergistic antimicrobial and selective cytotoxic potentials for biomedical advancements *J. Trace Elem. Med. Biol.* **81** 127325

[26] Tosyali O A, Allahverdiyev A, Bagirova M, Abamor E S, Aydogdu M, Dinparvar S, Acar T, Mustafaeva Z and Derman S 2021 Nano-co-delivery of lipophosphoglycan with soluble and autoclaved leishmania antigens into PLGA nanoparticles: evaluation of *in vitro* and *in vivo* immunostimulatory effects against visceral leishmaniasis *Mater. Sci. Eng.*C **120** 111684

[27] Ucar B, Acar T, Arayici P P and Derman S 2021 A nanotechnological approach in the current therapy of COVID-19: model drug oseltamivir-phosphate loaded PLGA nanoparticles targeted with spike protein binder peptide of SARS-CoV-2 *Nanotechnology* **32** 485601

[28] Wang Y, Zhai W, Cheng S, Li J and Zhang H 2023 Surface-functionalized design of blood-contacting biomaterials for preventing coagulation and promoting hemostasis *Friction* **11** 1371–1394

[29] Purr E, Marshall J and Smith J 2019 Preparation of PLGA nanoparticles encapsulated with fluorescent probe coumarin-6614875

[30] Zhang L, Xu Y, Cao W, Xie S, Wen L and Chen G 2018 Understanding the translocation mechanism of PLGA nanoparticles across round window membrane into the inner ear: a guideline for inner ear drug delivery based on nanomedicine *Int. J. Nanomed.* **13** 479

[31] Jiang N, Huang Q, Liu J, Liang N, Li Q, Li Q and Xie S-S 2018 Design, synthesis and biological evaluation of new coumarin-dithiocarbamate hybrids as multifunctional agents for the treatment of Alzheimer's disease *Eur. J. Med. Chem.* **146** 287–98

[32] Manidhar D, Rao K, Reddy N B, Sundar C S and Reddy C S 2012 Synthesis of new 8-formyl-4-methyl-7-hydroxy coumarin derivatives *J. Korean Chem. Soc.* **56** 459–63

[33] He Q, Liu J, Lan J-S, Ding J, Sun Y, Fang Y, Jiang N, Yang Z, Sun L and Jin Y 2018 Coumarin-dithiocarbamate hybrids as novel multitarget AChE and MAO-B inhibitors against alzheimer's disease: design, synthesis and biological evaluation *Bioorg. Chem.* **81** 512–28

[34] Xie S-S, Wang X-B, Li J-Y, Yang L and Kong L-Y 2013 Design, synthesis and evaluation of novel tacrine–coumarin hybrids as multifunctional cholinesterase inhibitors against Alzheimer's disease *Eur. J. Med. Chem.* **64** 540–53

[35] Kushwaha K, Kaushik N and Jain S C 2014 Design and synthesis of novel 2H-chromen-2-one derivatives bearing 1,2,3-triazole moiety as lead antimicrobials *Bioorg. Med. Chem. Lett.* **24** 1795–801

[36] Yee S W, Shah B and Simons C 2005 Synthesis and antimycobacterial activity of 7-O-substituted-4-methyl-2 H-2-chromenone derivatives vs *Mycobacterium tuberculosis* *J. Enzyme Inhibition Med. Chem.* **20** 109–13

[37] Derman S, Uzunoglu D, Acar T, Arasoglu T, Ucak S, Ozalp V C and Mansuroglu B 2020 Antioxidant activity and hemocompatibility study of quercetin loaded plga nanoparticles *Iran. J. Pharm. Res.: IJPR* **19** 424–35

[38] Amini Y, Amel Jamehdar S, Sadri K, Zare S, Musavi D and Tafaghodi M 2017 Different methods to determine the encapsulation efficiency of protein in PLGA nanoparticles *Bio-Med. Mater. Eng.* **28** 613–20

[39] Acar T, Arayıcı P P, Ucar B, Karahan M and Mustafaeva Z 2019 Synthesis, characterization and lipophilicity study of brucella abortus′ immunogenic peptide sequence that can be used in the future vaccination studies *Int. J. Pept. Res. Ther.* **25** 911–8

[40] Arasoglu T, Mansuroglu B, Derman S, Gumus B, Kocyigit B, Acar T and Kocacaliskan I 2016 Enhancement of antifungal activity of juglone (5-Hydroxy-1, 4-naphthoquinone) using a poly (D, L-lactic-*co*-glycolic acid)(PLGA) nanoparticle system *J. Agric. Food Chem.* **64** 7087–94

[41] Ucar B 2019 Synthesis and characterization of natural lanthanum labelled DOTA-peptides for simulating radioactive Ac-225 labeling *Appl. Radiat. Isot.* **153** 108816

[42] Ucar B and Acar T 2021 Macroaggregated albumin (MAA): production, size optimization, Eu (III) and Tb (III) complexes *J. Turkish Chem. Soc.*A **8** 209–16

[43] Madani F, Esnaashari S S, Bergonzi M C, Webster T J, Younes H M, Khosravani M and Adabi M 2020 Paclitaxel/methotrexate co-loaded PLGA nanoparticles in glioblastoma treatment: formulation development and *in vitro* antitumor activity evaluation *Life Sci.* **256** 117943

[44] Suri R, Neupane Y R, Mehra N, Nematullah M, Khan F, Alam O, Iqubal A, Jain G K and Kohli K 2021 Sirolimus loaded chitosan functionalized poly (lactic-co-glycolic acid) (PLGA) nanoparticles for potential treatment of age-related macular degeneration *Int. J. Biol. Macromol.* **191** 548–59

[45] Joshi D, Lan-Chun-Fung Y and Pritchard J 1979 Determination of poly (vinyl alcohol) via its complex with boric acid and iodine *Anal. Chim. Acta* **104** 153–60

[46] Sahu B, Pihlajamaa P, Zhang K, Palin K, Ahonen S, Cervera A, Ristimäki A, Aaltonen L A, Hautaniemi S and Taipale J 2021 Human cell transformation by combined lineage conversion and oncogene expression *Oncogene* **40** 5533–47

[47] Alkan F, Varlı H S, Demirbilek P D M, Kaplan P D E and Laçin P D N T 2020 A cationic stearamide-based solid lipid nanoparticle for delivering yamanaka factors: evaluation of the transfection efficiency *ChemistryOpen* **9** 1181

[48] Dinparvar S, Bagirova M, Allahverdiyev A M, Abamor E S, Safarov T, Aydogdu M and Aktas D 2020 A nanotechnology-based new approach in the treatment of breast cancer: biosynthesized silver nanoparticles using *Cuminum cyminum* L. seed extract *J. Photochem. Photobiol.* B **208** 111902

[49] Kumar K S, Kotra V, Kola P K, Devi C B P, Anusha N, Babu B H, Adil S F, Shaik M R, Khan M and Al-Warthan A 2021 ZnCl2 catalyzed new coumarinyl-chalcones as cytotoxic agents *Saudi J. Biol. Sci.* **28** 386–94

[50] de Araújo R S A, Carmo J d O d S, de Omena Silva S L, Costa da Silva C R A, Souza T P M, Mélo N B d, Bourguignon J-J, Schmitt M, Aquino T M d and Rodarte R S 2022 Coumarin derivatives exert anti-lung cancer activity by inhibition of epithelial–mesenchymal transition and migration in A549 cells *Pharmaceuticals* **15** 104

[51] Hrimla M, Oubella A, Laamari Y, Bahsis L, Ghaleb A, Itto M Y A, Auhmani A, Morjani H, Julve M and Stiriba S-E 2021 Click synthesis, anticancer activity, and molecular docking investigation of some functional 1,2,3-triazole derivatives *Biointerface Res. Appl. Chem.* **12** 7633–67

[52] Alam M M 2021 1,2,3-triazole hybrids as anticancer agents: a review *Arch. Pharm.* **355** e2100158

[53] Arasoglu T, Derman S, Mansuroglu B, Yelkenci G, Kocyigit B, Gumus B, Acar T and Kocacaliskan I 2017 Synthesis, characterization and antibacterial activity of juglone encapsulated PLGA nanoparticles *J. Appl. Microbiol.* **123** 1407–19

[54] Behnke M, Vollrath A, Klepsch L, Beringer-Siemers B, Stumpf S, A Czaplewska J, Hoeppener S, Werz O and

S Schubert U 2020 Optimized encapsulation of the FLAP/PGES-1 inhibitor BRP-187 in PVA-stabilized PLGA nanoparticles using microfluidics *Polymers* **12** 2751

[55] Sahoo S K, Panyam J, Prabha S and Labhasetwar V 2002 Residual polyvinyl alcohol associated with poly (D, L-lactide-co-glycolide) nanoparticles affects their physical properties and cellular uptake *J. Control. Release* **82** 105–14

[56] Gumus B, Acar T, Atabey T, Derman S, Sahin F and Arasoglu T 2020 The battle against biofilm infections: juglone loaded nanoparticles as an anticandidal agent *J. Biotechnol.* **316** 17–26

[57] Khanal S, Adhikari U, Rijal N P, Bhattarai S R, Sankar J and Bhattarai N 2016 pH-responsive PLGA nanoparticle for controlled payload delivery of diclofenac sodium *J. Funct. Biomater.* **7** 21

[58] Jusu S, Obayemi J, Salifu A, Nwazojie C, Uzonwanne V, Odusanya O and Soboyejo W 2020 Drug-encapsulated blend of PLGA-PEG microspheres: *in vitro* and *in vivo* study of the effects of localized/targeted drug delivery on the treatment of triple-negative breast cancer *Sci. Rep.* **10** 14188

[59] Shim H and Sah H 2020 Assessment of residual solvent and drug in PLGA microspheres by derivative thermogravimetry *Pharmaceutics* **12** 626

[60] Bhattacharjee S 2021 Understanding the burst release phenomenon: toward designing effective nanoparticulate drug-delivery systems *Ther. Deliv.* **12** 21–36

[61] Huang X and Brazel C S 2001 On the importance and mechanisms of burst release in matrix-controlled drug delivery systems *J. Control. Release* **73** 121–36

[62] Yoo J and Won Y-Y 2020 Phenomenology of the initial burst release of drugs from PLGA microparticles *ACS Biomater. Sci. Eng.* **6** 6053–62

[63] Fernandes C, Martins C, Fonseca A, Nunes R, Matos M J, Silva R, Garrido J, Sarmento B, Remiao F and Otero-Espinar F J 2018 PEGylated PLGA nanoparticles as a smart carrier to increase the cellular uptake of a coumarin-based monoamine oxidase B inhibitor *ACS Appl. Mater. Interfaces* **10** 39557–69

[64] Chen L, Lv Q, Cai J, Liang J, Liang Z, Lin J, Xiao Y, Chen R, Zhang Z and Hong Y 2023 Design, synthesis and anticancer activity studies of 3-(coumarin-3-yl)-acrolein derivatives: evidenced by integrating network pharmacology and vitro assay *Front. Pharmacol.* **14** 1141121

[65] Wu Y, Xu J, Liu Y, Zeng Y and Wu G 2020 A review on anti-tumor mechanisms of coumarins *Front. Oncol.* **10** 592853

[66] WHO 2024 Breast cancer (https://who.int/news-room/fact-sheets/detail/breast-cancer)

[67] Demkowicz S, Daśko M, Kozak W, Krawczyk K, Witt D, Masłyk M, Kubiński K and Rachon J 2016 Synthesis and biological evaluation of fluorinated 3-phenylcoumarin-7-O-sulfamate derivatives as steroid sulfatase inhibitors *Chem. Biol. Drug Des.* **87** 233–8

[68] Garro H A, Reta G F, Donadel O J and Pungitore C R 2016 Cytotoxic and antitumor activity of some coumarin derivatives *Nat. Product Commun.* **11** 1289–92

[69] Gkionis L, Kavetsou E, Kalospyros A, Manousakis D, Garzon Sanz M, Butterworth S, Detsi A and Tirella A 2021 Investigation of the cytotoxicity of bioinspired coumarin analogues towards human breast cancer cells *Mol. Diversity* **25** 307–21

[70] Gomaa M S, Ali I A, El Enany G, El Ashry E S H, El Rayes S M, Fathalla W, Ahmed A H, Abubshait S A, Abubshait H A and Nafie M S 2022 Facile synthesis of some coumarin derivatives and their cytotoxicity through VEGFR2 and topoisomerase II inhibition *Molecules* **27** 8279

[71] Song F, Huo X and Guo Z 2021 Anti-breast cancer potential of natural and synthetic coumarin derivatives *Curr. Top. Med. Chem.* **21** 1692–709

[72] Gurbuz İ, Gunbatan T, Bakar-Ates F, Hoti B, Duman H and Kilic C S 2023 The five ferulago species inhibited cell proliferation and induced apoptosis of A549, MCF-7, PC3 and SW480 cancer cells *in vitro 3 Biotech* **13** 122

[73] Sumi M, Nevaditha N and Kumari B S 2023 Nano zinc oxide-ruthenium (III) complex of novel coumarin derivative: synthesis, characterization, DNA cleavage, anticancer and bioimaging activities *Bioorg. Chem.* **136** 106555